

Fully Automated Method for Glaucoma Screening using robust Optic Nerve Head detection and unsupervised segmentation based Cup-to-Disc Ratio computation in Retinal Fundus Images

Amed Mvoulana^{a,*}, Rostom Kachouri^a, Mohamed Akil^a

^a*Gaspard-Monge Computer Science Laboratory, A3SI, ESIEE Paris, Université Paris-Est, Paris, France*

Abstract

Background and Objective: Visual impairment affects a significant part of the population worldwide. Glaucoma is one of these main causes, a chronic eye disease leading to progressive vision loss. Early glaucoma screening is an important task, allowing a slowing down of the pathology spreading and avoidance of irreversible vision damages. When manual assessment by experts suffers from disadvantages, exploiting the relevant Cup-to-Disc Ratio (CDR) feature as a structural indicator to assess the damage to the optic nerve head (ONH) is an efficient way for early glaucoma screening and diagnosis.

Methods: In this paper, we propose a new fully automated methodology for glaucoma screening and diagnosis from retinal fundus images. In order to allow eye examination in remote locations with limited access to clinical facilities, we focus in this work on the development of a computationally-efficient algorithm for further implementation on mobile devices. First, the method provides a robust optic disc (OD) detection method, combining a brightness criterion and a template matching technique, to effectively detect the optic disc (OD) even in the presence of bright lesions associated to pathological cases. Second, an efficient optic cup (OC) and optic disc (OD) segmentation is performed, using a texture-based and model-based approach. Finally, Cup-to-Disc Ratio (CDR) computation leads to glaucoma screening with a classification between healthy and glaucomatous patients.

Results: The proposed approach for glaucoma screening and diagnosis have been tested on the publicly available DRISHTI-GS1 dataset. Fifty retinal images are provided and labeled healthy or glaucomatous by trained specialists. The method achieves 98% of accuracy on final glaucoma screening and diagnosis, and excellent performance rates on evaluation metrics, outperforming the state-of-the-art CDR feature-based approaches.

Conclusions: We proposed a fully automated method for glaucoma screening and diagnosis from retinal images. Excellent performance was obtained on final screening, classifying healthy and glaucomatous subjects. As it effectively detects the presence of glaucoma, in a low-computational manner, the approach can be part of a mobile help-diagnosis system, to improve the final diagnosis by the specialist and develop widespread visual health programs.

Keywords: Glaucoma screening, Retinal images, Optic disc, Optic cup, Cup-to-Disc Ratio, Diagnosis.

* Corresponding author

Email address: amed.mvoulana@esiee.fr (Amed Mvoulana)

1. Introduction

Nowadays, visual impairment remains at the heart of important social challenges. About 253 million people worldwide suffer from vision loss, with 36 million affected by a complete and irreversible blindness (Bourne et al., 2017). Ocular pathologies are the main cause of visual impairment globally, as they generally lead to a loss of sight and can deteriorate to total blindness in some cases (Foster and Johnson, 1990). Chronic eye diseases are numerous (Varma et al., 2016), but recent studies show that moderate to severe visual impairment and blindness are often generated by four main ocular pathologies: cataracts, age-related macular degeneration, diabetic retinopathy, and glaucoma (Flaxman et al., 2017; Pascolini and Mariotti, 2012).

Glaucoma is a neurodegenerative eye disease, which alters the optic nerve head (ONH) (Quigley and Broman, 2006). This neuropathy is highlighted by a progressive lack of vision sensitivity, potentially leading to blindness at term. The early stage of glaucoma does not generate symptoms or changes to the visual field (Costagliola et al., 2009a). However, as the disease develops, a gradual narrowing of visual field occurs, starting from the periphery and extending towards the center. If glaucoma is not treated, the disease can lead to complete blindness (Bourne, 2007).

This paper deals with efficient early glaucoma screening and diagnosis, to ensure regular and more accessible eye tests. It is important to have early treatment to help stop the vision becoming severely affected. Glaucoma is known as affecting a significant part of the population worldwide, with more than 64 million cases reported in 2013 globally, and estimations reaching 80 million and 111.8 million cases respectively by 2020 and 2040 (Quigley and Broman, 2006; Tham et al., 2014). Although the presence of the disease is generally influenced by factors such as aging or ethnicity, glaucoma is unfortunately present for any age group or population type, and both developed and developing countries are targeted (Kingman, 2004). Glaucoma is also responsible for blindness in approximately 4.5 million people from all countries, making the neuropathy the second main cause of complete vision loss worldwide (12% of the total burden population) (Tham et al., 2014). Moreover, due to its asymptomatic feature at the early stage, 70 to 90% of the subjects suffering from glaucoma worldwide are unaware of the presence of the disease (Shen et al., 2008; Vijaya et al., 2005). Because glaucoma develops in silence, yields irreversible damages to vision, and for all of the reasons exposed above, it is critical to provide early screening and diagnosis. Then, this allows a more successful disease follow-up, in combination with a treatment able to slow down the spreading disease (Costagliola et al., 2009a,b).

In addition to visual field variation, two main tests allow glaucoma detection. The first consists in measuring the intraocular pressure (IOP) with a tonometer, and rating an abnormal high pressure rate. However, IOP measurement is not always a reliable and sufficient criterion for glaucoma assessment, as the presence of the disease does not necessarily induce an increase in IOP (Access Economics, 2008). The second is the assessment of the optic nerve head (ONH), the region in the retina where blood vessels converge and through which visual information transits to the brain. The ONH is composed of a bright circular region called the optic disc (OD), and inside the OD, a brighter region called the optic cup (OC) is apparent. In Fig. 1, two retinal images are presented, showing a sub-window around the ONH, with each of the OD and OC borders. Glaucoma goes with ONH appearance changes, as the OC region becomes more prominent as shown with both healthy (1) and glaucomatous (2) cases.

The evaluation of the changes in ONH appearance could generally be operated in two ways. The specialist

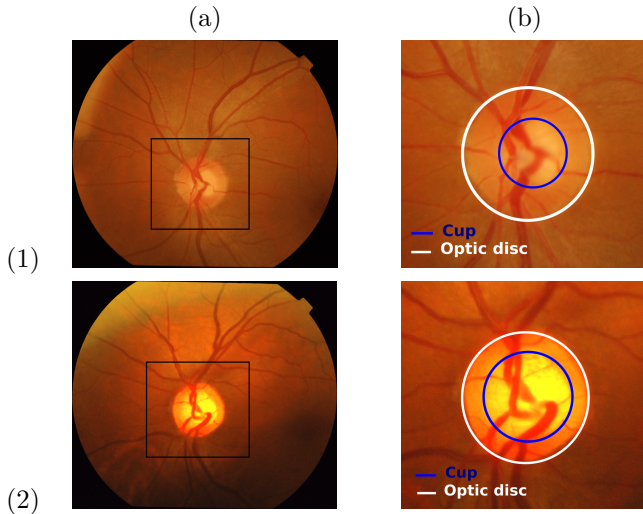


Figure 1: Example of healthy (1) and glaucomatous (2) retinal images: (a) Retinal image with framed optic disc (OD) region, (b) OD sub-image with OC and OD areas.

examination is the most common way for ONH assessment, nevertheless, it suffers from subjectivity, time-consuming and significant costs (Liu et al., 2009). Manual assessment can also be unpleasant for the patient (Bourne, 2007). The second way is more promising and efficient for glaucoma screening, and consists in a retinal image study (Abràmoff et al., 2010). Many works have been conducted in this direction, offering more accuracy on the final diagnosis, less workload for the specialist, and useful mass screening programs.

Detecting the presence of the disease from retinal images consists in assessing the ONH and the retinal nerve fiber layer (RNFL), by extracting indicators such as the Cup-to-Disc Ratio (CDR) (Wong et al., 2008), the Inferior Superior Nasal Temporal (ISNT) rule (Thakkar et al., 2017), the RNFL thickness (Medeiros et al., 2005), parapapillary atrophy (Jonas et al., 1992) or ONH hemorrhages Fingeret et al. (2005). When the other indicators are difficult to quantify without 3D-OCT imaging, the CDR appears as a relevant clinical feature for the assessment of ONH structural changes, as well as for detecting referable glaucomatous optic neuropathy from color fundus images (Foster et al., 2002; Cheng et al., 2013). Hence, exploiting the CDR contributes to the development of screening systems with 2-D dedicated snapshot devices and mobile platforms.

To implement CDR calculation for glaucoma screening, preliminary stages such as ONH detection, and both OC and OD areas segmentation are required (Singh et al., 2015b). However, as this medical framework requires the fulfillment of specific constraints, performing these stages is difficult. In particular, facing a huge variety of clinical cases is a challenging task, when non-robust OD detection or inaccurate OC and OD segmentation are ongoing issues (Cheng et al., 2013). Hence, in this disease screening context, overcoming limitations of existing methods at these respective stages is momentous.

Since early glaucoma diagnosis is primordial due to the irreversible vision damages caused during its progression, and to fill in the gaps of state-of-the-art screening methods, this paper proposes a new fully-automatic method for early glaucoma screening and diagnosis. Using 2-D retinal images, our proposed method calculates the CDR to carry

out the final diagnosis. Our contributions are: an efficient OD detection method, a new OC and OD segmentation method, CDR calculation and glaucoma screening. These contributions form part of a mobile computer-aided system for automatic screening of eye diseases we are developing (Elloumi et al., 2018). Hence, in parallel of the proposed method, a rigorous synthesis of its computational efficiency is made. The complete methodology allows an effective and reliable diagnosis-help system, which can be part of useful screening programs developing the universal access to the eye health (Blanckenberg et al., 2011; Bourouis et al., 2014).

The remainder of this paper is organised as follows. Section 2 presents an overview of the CDR-based state-of-the-art works for glaucoma screening and diagnosis. In section 3, the proposed method is explained. In section 4, materials are described and experimental results are shown. Section 5 discuss about the proposed methodology. Finally, the conclusion and perspectives appear in section 6.

2. CDR-based glaucoma screening related works

Three main clinical techniques lead to glaucoma screening: assessment of the intraocular pressure with a tonometer, assessment of the visual field with static and kinetic tests, and assessment of the optic nerve head (ONH) with recent devices such as optical coherence tomography (OCT) or scanning laser ophthalmoscope (SLO) (Lim et al., 2012). Nevertheless, these techniques suffer from disadvantages such as operator-dependence or significant costs (Liu et al., 2009). To address these limitations, recent studies have proposed automated methods for glaucoma screening and diagnosis from retinal images (Bock et al., 2010; Singh et al., 2015b). These approaches tend to be more accurate in final disease screening, while being less expensive and contributing to the development of widespread glaucoma screening programs (Abràmoff et al., 2010).

Since the OC excavation is the first visible sign of the presence of glaucoma, the retinal image study for glaucoma assessment consists in the evaluation of the ONH morphological changes. Hence, different parameters such as diameter and area of the OC and the OD, or the area of the Neuro-Retinal Rim (NRR) need to be retrieved (Hu et al., 2017). Then, clinical features such as the Inferior-Superior to Nasal-Temporal (ISNT) rule (Thakkar et al., 2017) or the cup-to-disc ratio (CDR) (Wong et al., 2008) are employed to assess glaucoma. Among these different features, the CDR is a reliable and often-used clinical feature for early glaucoma screening and diagnosis (Bourne, 2007). It represents the ratio between the OC and the OD, according to one of the extracted parameters (diameter or area). The CDR value increases as the disease develops, and becomes higher than around 0.6-0.7 when the patient suffers from a greater risk of developing glaucoma (Abràmoff et al., 2010). Thereby, the CDR value helps to monitor the progression of glaucoma over time, to finally screen the disease early (Wong et al., 2008).

To compute the CDR from retinal images, a joint OC-OD segmentation is required (Cheng et al., 2013). Accurate segmentation is mandatory to correctly calculate the CDR and finally classify healthy and glaucomatous subjects Singh et al. (2015b). In the context of the project we are carrying out, the existing segmentation methods for glaucoma screening are generally ranged into two different approaches: supervised approaches and unsupervised approaches.

In supervised approaches, image-level features are extracted from the fundus images (Wong et al., 2010). Then, a set of retinal images with the manual boundaries of the OC and the OD is used to train a specific classifier then detect the

OC and OD areas with the computed features. For example, Chakravarty and Sivaswamy (2017) proposed a boundary-based method for OC-OD segmentation, where several image features such as color gradients and depth estimations are retrieved from retinal images. A Conditional Random Field is formulated, using an energy minimization criteria to fit on the boundaries. Then, these features are used to feed a support vector machine (SVM) classifier during the learning phase. After obtaining the OC and OD boundaries, CDR calculation is finally performed to lead to glaucoma screening. In the same way, Cheng et al. (2013) extracted both OC and OD areas using a superpixel classification-based method. A simple linear iterative clustering (SLIC) superpixel algorithm (Achanta et al., 2012) is operated on the OD sub-image. Then, five color channel maps and their associated histograms are generated, as well as 18 center surrounded statistics maps to bring a more textural information. The features of each superpixel are used as the inputs of an SVM algorithm, to classify each superpixel as part of the OC or the OD. After finding each area, the CDR is computed to assess glaucoma. As a major advantage, the supervised approaches tend to efficiently segment the OC and OD areas. However, a supervised learning phase is required to perform the segmentation, inducing time-consuming or large data requirements when the precise ground-truth labelling is a tedious task. Moreover, the choice of the image features (color, texture, energy, etc.) used to train the segmentation classifier is difficult. These aspects of the supervised approaches may be an obstacle according to our purpose, where a low-computational algorithm is required.

Unsupervised approaches provide OC and OD segmentation without any learning phase. Among unsupervised state-of-the-art approaches, image processing techniques such as image thresholding or morphological operators have been frequently used to segment both OC and OD areas (Aquino et al., 2010; Stapor et al., 2004). Then, CDR calculation leads to glaucoma screening, as a binary classification between healthy and glaucomatous patients is generally operated (Singh et al., 2015b). For example, Singh et al. (2015a) associated image pre-processing techniques, such as binarization and morphological operations to finally compute the CDR with the found OC and OD areas. Thereafter, a compensated CDR value allows to classify the retinal image as healthy or suspicious. Also, Guerre et al. (2014) proposed a fully-automated method for glaucoma detection, based on basic processing techniques. A preprocessing phase is operated to manage with uneven illumination or eventual noise. After, a blood vessels' mask generated with an Isotropic Undecimated Wavelet Transform (IUWT) is combined with an adaptive thresholding algorithm to segment the OC and OD areas. Then, the CDR is computed as a feature to assess glaucoma. In these methods, simple and effective algorithms are used to extract the desired areas, going with less computationally complex algorithms for glaucoma screening. However, since the segmentation task is arduous due to blood vessels occlusions, or variable imaging acquisitions such as weak illumination or low contrast, these algorithms may not be sufficient and provide underestimated extracted areas. Hence, a lack on segmentation performance is noticed, what influences the obtained CDR value and final glaucoma screening. To improve the segmentation accuracy using these low-complex unsupervised algorithms, a strategy consists in the use of model-based algorithms to fit on the boundaries. In this way, some methods have used active contours (Joshi et al., 2011). For example, Wong et al. (2008) formulated an approach mainly based on a variational level-set technique to detect the OC and OD borders. A thresholding method is applied to initialize the contour. Then, the CDR is computed from the detected areas to assess glaucoma. The active contour

based methods slightly improve the segmentation accuracy, compared to the methods based on image processing techniques only. However, the choice of the active contours parameters is challenging, such as the initialization around the OD or the contour deformation (with energy-based features for example), to effectively converge and fit on the desired boundaries. To avoid the use of deformable contours, some methods have used the circular Hough transform (Pedersen, 2007) to model the OC and OD boundaries. For example, Priyadharsini et al. (2018) performed image processing techniques such as channel extraction or histogram equalization, to emphasize the intended areas in the retina. Then, circular Hough transform is operated to detect the OD boundaries. Next, morphological operations are subsequently used to detect the OC area. As a major advantage compared to active contours, circular Hough transform requires a few parameters to effectively find the OC and the OD, while providing a good computationally-efficient property against accuracy on the final segmentation result. In this work, we follow this direction, hence, we combine the Hough transform with a prior detection of the OD surroundings to answer to the drawbacks of the existing methods and detect the borders in a precise manner for further glaucoma screening.

In this paper, we propose then a new method for glaucoma screening and diagnosis (see section 3) from fundus images. Firstly, an OD detection approach is performed, allowing to detect the area of interest around the OD, even in the eventual presence of bright lesions in pathological cases (see section 3.1). Here, a brightness criterion merged to a template matching technique is operated to effectively detect the disc, and extract the sub-window around it. Secondly, the OC and OD segmentation is operated using an unsupervised texture-based method, to effectively detect the pixels belonging to the desired areas without the computation of a complex learning phase. Then, a model-based boundary fitting method is subsequently applied, to improve segmentation performance (see section 3.2). CDR calculation (see section 3.3) is finally used for glaucoma screening (see section 3.4). The approach performance on final screening and diagnosis is evaluated and compared to the existing methods for glaucoma screening. Our proposed pipeline (see Fig. 2) improves over the current state-of-the-art, while performing low-complex unsupervised algorithms.

3. Proposed Method

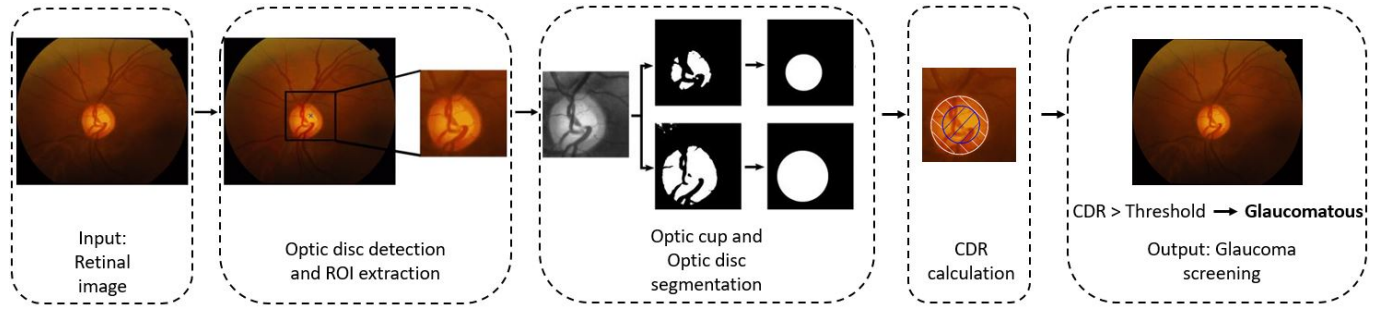


Figure 2: Flowchart of the proposed method for glaucoma screening and diagnosis.

The method for early glaucoma screening and diagnosis consists of the following main stages: optic disc (OD) detection and region-of-interest (ROI) extraction around the OD (see section 3.1), optic cup (OC) and optic disc (OD) segmentation (see section 3.2), cup-to-disc ratio (CDR) calculation (see section 3.3) and glaucoma screening

(see section 3.4). A flowchart of the proposed method is presented in Fig. 2. In this section, we also introduce the pseudo-codes of the proposed method for glaucoma screening, according to each stage of the algorithm. The written codes allow to stretch out the structure of the program, provide a complete understanding of the role of each function and create a bridge between the method and its implementation (see Algorithms 1, 2, 3, 4 and 5).

3.1. Optic disc detection and ROI extraction

OD detection is a primordial step in computer-aided systems, providing an essential contribution for the screening of diabetic retinopathy (DR) or glaucoma (Chrásťek et al., 2005; Walter et al., 2002). However, automatic OD detection is a challenging task, particularly in the presence of bright lesions going with various ocular pathologies such as diabetic retinopathy, Coats disease, etc. (Xiong and Li, 2016). In Fig. 3, an example of this mentioned drawback is outlined. These bright lesions are not related to the glaucoma case, as glaucoma generates structural changes within the ONH only. Nevertheless, to ensure the glaucoma screening process, it is mandatory to ensure a robust OD detection, even if subjects eventually suffer from other diseases inducing the apparition of these bright lesions. Hence, we can reliably conduct glaucoma screening even in the presence of other ocular pathologies.

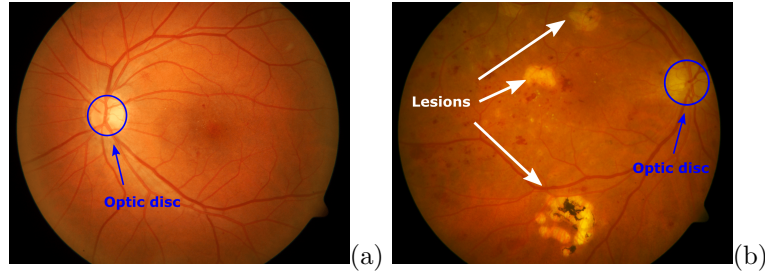


Figure 3: Example with different retinal images: (a) retinal image without any lesion, (b) retinal image with large lesions, associated to a diabetic retinopathy.

Many approaches have been proposed in the literature for OD detection. They can be divided in three main categories: approaches based on vascular tree extraction, approaches based on OD appearance (brightness/circularity), and approaches based on OD template matching.

The approaches based on the vascular tree tend to extract the vessel structure and exploit its convergence to the OD center (Mahfouz and Fahmy, 2010; Youssif et al., 2008; Zhang and Zhao, 2016). Foracchia et al. (2004) exploited the vessels direction using a geometrical model of the vascular structure, to detect the OD. Soares et al. (2016) used the orientation of the four main vessels by computing cumulative sum fields, leading to OD center localization. These methods tend to be robust to the changes on OD appearance, and efficiently detect the OD in both healthy and pathological cases. However, a recent study (Ben Sayadia et al., 2018) showed that these approaches lead to an important computation complexity, as it requires a complete extraction of the retinal vascular tree. Hence, it is inappropriate to our study where the computational efficiency is an important parameter to consider. Also, the complete extraction of the vessels is challenging with obstructive lesions.

To avoid the extraction of the vascular tree, some methods used the OD features such as brightness or circularity. It is the most intuitive feature to exploit, while bringing important information for OD detection. For example, Pourreza-Shahri et al. (2014) used the Radon transform (Radon, 1986) on several angles to detect bright and circular areas. Also, Hashim et al. (2015) proposed a combination between morphological operations, and Gaussian differences that improves the edges visibility, to finally get the OD boundaries. Rahebi and Hardalaç (2016) performed a high points intensity research, using a Firefly algorithm (Yang, 2010). In the work by Giraddi et al. (2017), a thresholding method is operated to extract bright areas, and an active contour algorithm lead to OD extraction. These methods tend to exhibit good results in healthy retinal images. However, they often suffer from some weaknesses with the presence of great-intensity lesions, and lower accuracy is observed compared to the methods based on the vascular tree (see Fig. 3 (b) and Fig. 4 (a)).

OD Template Matching approaches tend to detect the OD in the image, from previously-defined OD models. The most relevant example of this approach is the work by Dehghani et al. (2012), which consists firstly of the creation of histogram models of the OD. Second, a scanning of the retinal image allows to detect the OD using a sliding sub-window and the computed model. On the same principle, Wankhede and Khanchandani (2016) built an OD histogram model by estimating the OD radius, and computed a similarity coefficient between the OD histogram and current sliding sub-window to finally detect the OD final location. Here, the main advantage compared to other approaches is that not any segmentation step is required. Also, these methods do not suffer from previously-exposed limitations, where they strongly depend on the OD appearance or on a complete extraction of the vessels. However, the main disadvantage is the entire image path to find the OD location, which can lead to eventual matching errors or more important computation times.

Algorithm 1 OD detection

```

1: Input: retinal image  $I$ 
2: Output: OD sub-image  $OD\_crop$ 
3: function OD_DETECTION( $I$ )
4:    $centroids \leftarrow \text{DETECT\_BRIGHT\_REGIONS}(I)$                                  $\triangleright$  see Algorithm 2
5:   if  $\text{length}(centroids) > 1$  then
6:      $center \leftarrow \text{TEMPLATE\_MATCHING}(od.hist.template, centroids, image)$            $\triangleright$  see Algorithm 3
7:   else
8:      $center \leftarrow centroids[0]$ 
9:    $OD\_crop \leftarrow I[center, S]$ 
10:  return  $OD\_crop$ 

```

We take into account each approach and its limitations and propose a new efficient and robust method for OD detection in retinal images (see Algorithm 1). Several contributions are made in this work to provide a non computationally-complex method, while detecting the OD even in the presence of lesions. First, we detect the brightest regions in the retinal image (see section 3.1.1). Second, to effectively detect the final OD location among eventual bright lesions, a template matching technique is computed only on the found bright points (see section 3.1.2). Finally, a sub-image

around the OD is extracted.

3.1.1. Detection of bright regions

Our approach for the detection of bright regions is composed of the following steps: preprocessing, thresholding, distance map computation and selection of the maximum points on the distance map (see Algorithm 2).

Algorithm 2 Detection of the bright regions

```

1: Input: retinal image  $I$ 
2: Output: list of coordinates centroids
3: function DETECT_BRIGHT_REGIONS( $I$ )
4:    $I \leftarrow \text{HISTOGRAM\_EQUALIZATION}(\text{green\_level}(I))$ 
5:    $\text{binary} \leftarrow \text{OTSU\_THRESHOLDING}(I)$ 
6:    $\text{map} \leftarrow \text{DISTANCE\_MAP}(\text{binary})$ 
7:   for all  $p$  in  $\text{map}$  do
8:     if  $p > \max(\text{map})/2$  then
9:        $\text{maxima}[i, j] \leftarrow 255$ 
10:    else
11:       $\text{maxima}[i, j] \leftarrow 0$ 
12:    for all  $\text{convex\_component}$  in  $\text{maxima}$  do
13:       $c \leftarrow \text{CENTER\_OF\_MASS}(\text{convex\_component})$ 
14:       $\text{centroids} \leftarrow \text{centroids.append}(c)$ 
15: return  $\text{centroids}$ 

```

First, since retinal images may suffer from some lighting defects, non-uniform intensity variations or poor contrast, a prior preprocessing step is computed (Hashim et al., 2015; Youssif et al., 2008). If color fundus images, green channel is extracted, since it provides the highest contrast and a better highlighting of the brightest regions in the retinal image (Inoue et al., 2006). Then, in order to enhance contrast and emphasize the visualization of the retinal structures, an adaptive histogram equalization method (CLAHE) (Pizer et al., 1987) is applied, offering a local-based contrast enhancement (see Fig. 4 (b)).

Thereafter, in order to efficiently separate needed bright regions to other retinal structures such as blood vessels or background, a binary thresholding method is operated. In this way, many methods exist and are applied for retinal image study, with global or local techniques (Soares et al., 2016). Among this thresholding techniques, Otsu's local thresholding method appears as a best choice for this presented task, allowing good managing with uneven illumination when acquiring fundus images (Abràmoff et al., 2010). Nevertheless, we notice that applying Otsu's method may lead to an inappropriate binarization in some extreme cases, separating the vascular tree from the other retinal components. To solve this problem, we set the obtained Otsu's threshold value T_O to $(\frac{4}{3}) \times T_O$ to ensure the thresholding operation match with our context of detecting bright regions (see Fig. 4 (c)). An example with the applied function to separate the bright regions from background is presented in Fig. 5.

Then, to compute a derived metric representation of the obtained binary image, and emphasize all brightest areas, an intensity map is implemented. Here, the Euclidean distance map on the output binary image is applied: each white

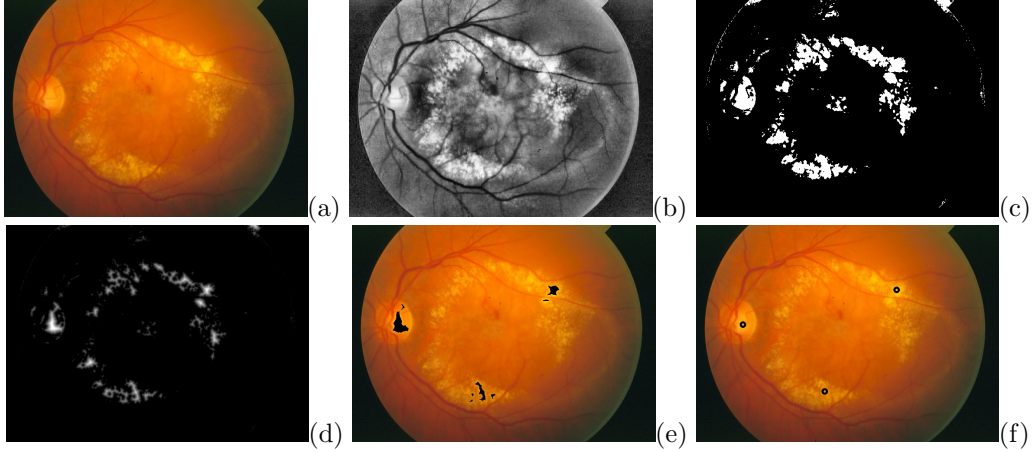


Figure 4: Detection of bright regions on a retinal image (STARE database): (a) Original retinal image with great-intensity lesions, (b) preprocessed image, (c) binary image, (d) distance map, (e) maximum points on distance map , (f) center approximation.



Figure 5: Example with applied thresholding method: (a) contrast-enhanced image, (b) binary image using Otsu's method, (c) final binary image applying supplement threshold value.

pixel is associated with its distance to the nearest black pixel (Xiong and Li, 2016) (see Fig. 4 (d)).

Afterwards, in order to select the largest bright regions from the distance map, an adaptive selection is applied by extracting the interval $I = [\frac{1}{2} \times max_{DT}; max_{DT}]$ depending on the maximum value max_{DT} in the obtained distance map (see Fig. 4 (e)). Finally, each area is replaced by its centroid, being a representative point of area location (see Fig. 4 (f)).

After these steps (preprocessing, thresholding, distance map computation, maximum points on distance map, center approximation), brightest regions are detected, each represented by its centroid as location point. In healthy cases, since no bright lesions are apparent, only one point is found then corresponds to the OD location. However, in the presence of bright lesions associated to pathological cases, other bright points may be detected. In this case, it is primordial to propose a complementary step for OD recognition, providing an efficient way to detect the OD location among eventual bright lesions. Section 3.1.2 presents the adopted strategy.

3.1.2. Template Matching

Here, we propose a template matching technique to detect the OD even in the eventual presence of bright lesions in the retinal image. The technique is in accordance with the strategy followed in Dehghani et al. (2012); Wankhede and Khanchandani (2016). The two main steps of this technique are the creation of the OD histogram templates (see

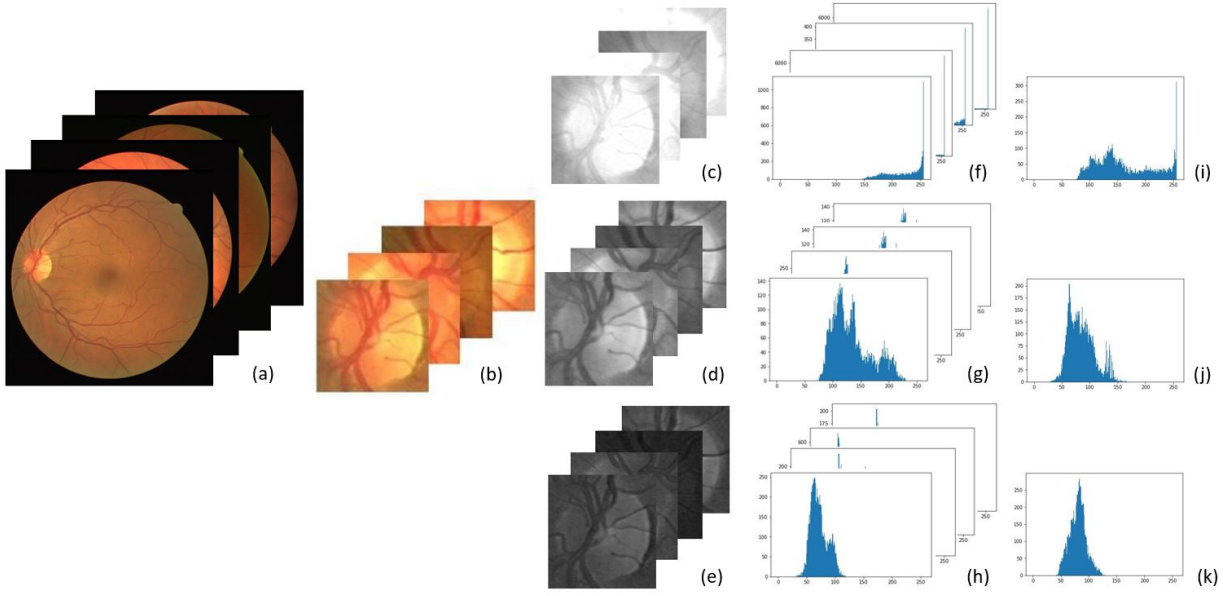


Figure 6: Creation of the OD template, from the chosen retinal images to the template histograms (DRIVE database): (a) retinal images, (b) sub-windows around the OD, (c) red channel sub-windows, (d) green channel sub-windows, (e) blue channel sub-windows, (f) red channel histograms, (g) green channel histograms, (h) blue channel histograms, (i) mean red channel histogram, (j) mean green channel histogram, (k) mean blue channel histogram.

section 3.1.2.1) and the matching among the found bright regions (see section 3.1.2.2), finally leading to OD detection.

3.1.2.1. Creation of the OD histogram templates. Here, we create the histogram templates associated to each evaluation database. We exploit well-known and often used databases for the evaluation of OD detection methods, such as DRIVE (Staal et al., 2004), STARE (Hoover et al., 1998), DIARETDB0 (Kauppi et al., 2006), DIARETDB1 (Kälviäinen and Uusitalo, 2007) or ROC (Niemeijer et al., 2010). Since a representative OD model is required, several retinal images are chosen in the respective database (see Fig. 6 (a)). Similarly to Dehghani et al. (2012); Osareh et al. (2003), we make sure to use images with different OD appearance, to build the most robust OD model. For the following, each detailed step is applied to each chosen image.

Firstly, since an OD model is needed, a sub-image around the OD is selected. Here, a semi-automatic extraction method is performed, using a manually-defined OD center and estimating automatically the OD radius (Wankhede and Khanchandani, 2016). Indeed, the OD radius (in pixels) in a retinal image depends on the intrinsic Field-Of-View (FOV) parameter of the used camera, and the resolution of the image. Let N_{FOV} be the number of pixels in the FOV, and A_{FOV} the specific area in the FOV. The image footprint, I_{FP} , is defined as:

$$I_{FP} = \frac{A_{FOV}}{N_{FOV}} \quad (1)$$

So, the OD radius in pixels is calculated using the average human OD diameter $D_{OD} \approx 1.85mm$ (Wankhede and

Khanchandani, 2016). Using (1), the OD radius R_{OD} is defined as:

$$R_{OD} = \sqrt{\frac{(D_{OD}/2)^2}{I_{FP}}} \quad (2)$$

Using (2), automatic estimation of the square length l of the sub-image is defined as:

$$l = 2 \times R_{OD} + \Delta \quad (3)$$

with $\Delta = 1/3 \times R_{OD}$ to make sure to contain all the OD in the sub-image.

Dataset	A_{FOV} (mm^2)	Image size (N_{FOV})	R_{OD}	ROI (l)
DRIVE (Staal et al., 2004)	124.8	768 x 584	55	75
STARE (Hoover et al., 1998)	235.6	605 x 700	125	165
DIARETDB0 (Kauppi et al., 2006)	54.3	1500 x 1152	165	220
DIARETDB1 (Kälviäinen and Uusitalo, 2007)				
ROC (Niemeijer et al., 2010)	37.4	1386 x 1391	210	280

Table 1: R_{OD} values for several retinal images on the publicly available datasets, and computed ROI square length.

Table 1 presents the value of the obtained OD radius obtained from different image databases, using described parameters and formulas. Using these results and setting up the OD center, the approximation of the OD radius allows to extract the sub-image around the OD from each selected images (see Fig. 6 (b)).

Then, in order to exploit all the information provided by the color image, the three red, green and blue channels are extracted from the sub-image. If the method for OD detection is applied on gray-scale images, we use the gray-scale channel only (see Fig. 6 (c), (d) and (e)).

Afterwards, the histogram for each extracted sub-image is computed then registered, as it provides relevant trend of intensity values present in the calculated OD sub-image (see Fig. 6 (f), (g) and (h)).

Finally, we gather the resulting histograms of each chosen images for the template creation, and compute the associated mean histogram to each extracted channel. Here, three final histogram templates are obtained for color images, among the chosen images (see Fig 6 (i), (j), (k)). Otherwise, in gray-scale images, one histogram is obtained, corresponding to the mean histogram computed on the gray-scale sub-images.

3.1.2.2. Matching. After the creation of the OD histogram templates, matching phase is applied on the found bright regions (see section 3.1.1) to detect the final OD location (see Algorithm 3).

First, from the position of each detected bright region in the image (see section 3.1.1), we extract a surrounding sub-image centered on each detected point position. The square length is automatically set using the same technique as described in Eq. (3).

After, if exist, the channels are separated, giving for each point position three sub-images in color images or one sub-image in gray-scale images. Then, the histogram of each sub-image is computed as described in section 3.1.2.1.

Algorithm 3 Template matching

```
1: Input: retinal image  $I$ , list of coordinates  $centroids$ , histogram template  $od\_hist\_template$ 
2: Output: Coordinates of the OD  $OD\_coordinates$ 

3: function TEMPLATE_MATCHING( $I$ )
4:   for all  $c$  in  $centroids$  do
5:      $crop \leftarrow image[c, s]$                                  $\triangleright$  crop around the point  $c$ , with square size  $s \times s$ 
6:      $hist \leftarrow CALCUL\_HIST(crop)$ 
7:      $corr \leftarrow CORRELATION(hist, od\_hist\_template)$ 
8:     if  $corr > max\_corr$  then
9:        $max\_corr \leftarrow corr$ 
10:       $center \leftarrow c$ 
11:    return  $OD\_coordinates$ 
```

Next, to launch template matching and final OD detection, cross-correlation method is performed between the histogram templates, and the associated histograms to each bright point. The Correlation Similarity Index between two histograms a and b is defined as:

$$c = \frac{1}{(1 + \sum_n (a_k - b_k)^2)} \quad (4)$$

where k denotes the histogram bins, and for two similar histograms, $\sum_n (a_k - b_k)^2 \approx 0$ and $c \approx 1$.

For gray-scale images, we use (4) to compute the correlation between the two gray-scale histograms. For color images, we use a weighted sum function. The correlation between the histograms is defined then as:

$$C(i, j) = \alpha \times c_R + \beta \times c_G + \gamma \times c_B \quad (5)$$

with (i, j) the coordinates of the central window point, c_λ the Correlation Similarity Index of the histograms of each color channel $\lambda = R, G, B$, and α, β, γ positive weights allowing to master the influence of each channel. Since the green channel provides a better contrast, when blue and even more red channels may suffer from non-uniform OD illumination or more artifacts (Hashim et al., 2015), weights are defined as $\alpha = 0.5$, $\beta = 2$ and $\gamma = 1$ to enhance green channel influence (Dehghani et al., 2012).

Finally, the retained OD location point is associated to the window with the highest correlation value between the corresponding histogram and the employed template one, among all found bright points (see section 3.1.1).

An example of the template matching result is illustrated in Fig. 7, with the found bright regions (see Fig. 7 (a)), and the final OD location result after applying the template matching. An extraction of the sub-window around the OD location represents the region-of-interest (ROI) (see Fig. 7 (c)).

We note that our new proposed OD detection method ensures a robust and effective ROI extraction around the OD, even in the potential presence of bright lesions going with pathological cases. To compute the CDR and lead to glaucoma screening from the extracted ROI sub-image, a joint OC-OD segmentation method is proposed in section 3.2.

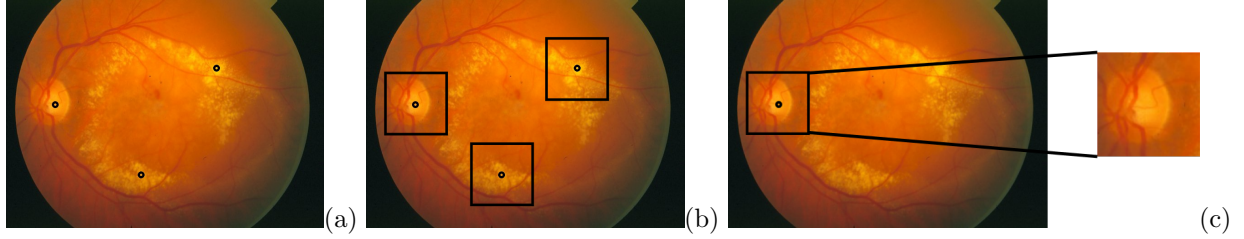


Figure 7: Template Matching on detected bright points: (a) image with the detected points, (b) image with framed neighborhood around the points, (c) final OD location point with the extracted ROI.

3.2. Optic cup and optic disc segmentation

Algorithm 4 OC and OD segmentation

```

1: Input: OD sub-image  $OD\_crop$ 
2: Output: OC segmentation  $optic\_cup$ , OD segmentation  $optic\_disc$ 
3: function OC_OD_SEGMENTATION( $OD\_crop$ )
4:    $gray\_level \leftarrow GRAY\_LEVEL(OD\_crop)$ 
5:    $image\_kmeans, label, centers \leftarrow K\text{-MEANS}(gray\_level, 4)$ 
6:    $maximum \leftarrow max(centers)$ 
7:    $second \leftarrow second(centers)$ 
8:    $first\_label \leftarrow label[maximum]$ 
9:    $second\_label \leftarrow label[second]$ 
10:  for all  $p$  in  $image\_kmeans$  do
11:    if  $label(p) == first\_label$  then
12:       $optic\_cup[p] \leftarrow 255$ 
13:    else if  $label(p) == second\_label$  then
14:       $optic\_disc[p] \leftarrow 255$ 
15:  for  $image$  in  $optic\_cup, optic\_disc$  do
16:     $circle \leftarrow CIRCULAR\_HOUGH\_TRANSFORM(image)$ 
17:    for  $p$  in  $image$  do
18:      if  $p$  in  $circle$  and  $p == 0$  then
19:         $p \leftarrow 255$ 
20:      else if  $p$  outside  $circle$  and  $p == 255$  then
21:         $p \leftarrow 0$ 
22:  return  $optic\_cup, optic\_disc$ 

```

OC and OD segmentation plays a key role in many computer-aided diagnosis systems in ophthalmology. It is an essential task to identify ocular conditions such as glaucoma or diabetic retinopathy (Cheng et al., 2013; Nugraha and Soesanti, 2016). Nevertheless, the segmentation of the OC and even more the OD is difficult, since they have not well-defined boundaries.

As viewed with the related works for glaucoma screening (see section 2), existing methods for OC and OD segmentation are ranged into supervised or unsupervised approaches. When supervised methods require a constraining training phase, with important resources and computationally-complex algorithms, unsupervised approaches bring a

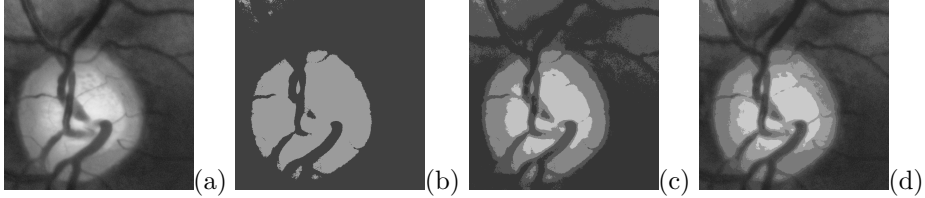


Figure 8: Applied clustering method on input OD sub-image: (a) OD gray-level sub-image, (b) K-means with $K=2$, (c) K-means with $K=4$, (d) K-means with $K=8$.

slighter computation cost. Hence, we follow this lane to deliver an easy-to-perform method from 2-D retinal images. However, a lack on the segmentation performance is noticed with existing unsupervised approaches, what influences the obtained CDR value and final glaucoma screening.

To overcome the lacks of existing methods, we present a new effective approach for joint OC-OD segmentation (see Algorithm 4). Here, the main challenge is to establish a trade-off between segmentation rate and computation efficiency. In this way, we firstly perform a texture-based method, relying on the intensity aspect of the areas, to give a prior segmentation of the required areas. Secondly, a model-based boundary fitting method allows to properly detect the edges, smoothing the borders and improving the segmentation result. Starting from the gray-level sub-image of the OD (see section 3.1), the proposed segmentation method consists of the two following steps: texture-based pixel classification (see section 3.2.1) and model-based boundary fitting (see section 3.2.2).

3.2.1. Texture-based pixel classification

To compute the joint OC-OD segmentation, a texture-based strategy is firstly operated to classify each pixel among a retinal structure. Here, an unsupervised clustering approach is adopted, to avoid a learning phase and its resource-intensive process. K-means clustering is a well-known classification algorithm, which consists in grouping similar points following a nearness criterion (MacQueen et al., 1967). A well-defined distance function $D(x, y)$ and a positive integer K are the two parameters for K-means clustering. Frequently, the used distance D is the Euclidean distance (Kodinariya and Prashant, 2014). The value K is often related to the context, and corresponds to the number of clusters needed to find. From K cluster centroids, using the distance D , each data point is allocated to the cluster of the nearest centroid.

In this segmentation context, where texture is a relevant feature to extract and show off each retina component, the K-means clustering algorithm is employed using an intensity-based nearness criterion. Thus, this approach allocates each area of the retinal sub-image among K clusters following its gray-level. Since the main retinal components are the OC, the OD, the background and the blood vessels, a fixed value $K = 4$ is selected. Fig. 8 presents an example of the applied clustering method with different values of K . For $K = 2$ (see Fig. 8 (b)), we notice that there is a separation between the entire OD area and the retinal area, without a distinction between the OC and the OD. Inversely, too much areas appear for $K = 8$ (see Fig. 8 (d)). This result strengthens the choice of the value $K = 4$ (see Fig. 8 (c) and Fig. 9 (b)).

Then, since the OC and the OD are the greater-intensity areas in the sub-image, they are both associated to the

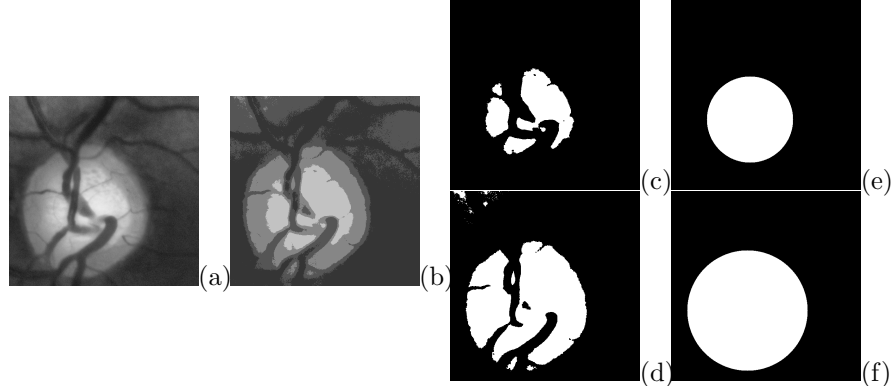


Figure 9: Example with OC and OD segmentation method steps: (a) sub-image around the OD, (b) k-means with $K=4$, (c) OC extraction and thresholding, (d) OD extraction and thresholding, (e) final OC segmentation, (f) final OD segmentation.

two greater-intensity clusters. Thus, the cluster with the greater intensity corresponds to the OC area, when the second greater-intensity cluster corresponds to the Neuro-Retinal Rim (NRR) area. The gathering of each found area forms the OD. From this result, to obtain an uniform rendering, the output K-means image is further thresholded twice using respectively the greater-intensity and the second greater-intensity (see Fig. 9 (c) and (d)).

3.2.2. Model-based boundary fitting

From the segmentation result after applying the pixel classification (see section 3.2.1), some gaps are apparent on both OC and OD areas because of the presence of the blood vessels converging into the OD. Also, some noise along the borders is present, which can degrade the segmentation accuracy. Since morphological operators may not always fill in these gaps, with variable blood vessels thicknesses, a strategy consists in computing a fitting of both OC and OD boundaries. This fitting strategy also allows to smooth the OC and OD borders, while improving the segmentation accuracy (Wong et al., 2010). Here, since regions of interest are known for their rather circular feature, circular Hough transform (Pedersen, 2007) is performed (Aquino et al., 2010; Zhu and Rangayyan, 2008). After detecting the OC and OD borders by applying the circular Hough transform, we consider that each pixel inside the circle is part of the final segmentation, and final segmentation is unaltered by the presence of the blood vessels (see Fig. 9 (e) and (f)).

Within our new proposed method for joint OC-OD segmentation, OC and OD areas are extracted on the retinal image. Texture-based feature followed by model-based fitting allow to effectively segment each desired area. For the further, CDR calculation is proposed in section 3.3 for glaucoma screening.

3.3. CDR calculation

Many methods have exploited the relevant cup-to-disc ratio (CDR) feature for early glaucoma screening. The CDR is a reliable clinical feature to estimate the structural changes of the ONH, and assess an early-occurring glaucoma. In this context, two different forms of CDR exist and are exploited in state-of-the-art approaches, both assessing the cupping of the ONH and being factors of glaucoma presence risk (Wong et al., 2008). First, the diameter-based CDR consists in computing the ratio between the vertical (or horizontal) diameter of each OC and OD regions. This feature

have been extensively used in state-of-the-art methods, well-accepted by specialists (Cheng et al., 2013). Second, recent methods for early glaucoma screening and diagnosis have used the area-based CDR, CDR_{area} (Nugraha and Soesanti, 2016; Priyadharsini et al., 2018). CDR_{area} consists in the ratio between the area of each OC and OD regions:

$$CDR_{area} = \frac{OC_{area}}{OD_{area}} \quad (6)$$

where each area is defined as the number of pixels in each respective region. Area-based CDR provides a 2-D feature-based measurement allowing to assess the structural changes of the ONH (Maldhure and Dixit, 2015). Hence, we adopt this choice as it appears as a better criteria for our glaucoma screening context aiming to measure the cupping portion onto the ONH. In this way, from each OC and OD segmentation (see section 3.2), we calculate their respective area (number of white pixels), to finally compute the area-based CDR and conduct to glaucoma screening (see Algorithm 5).

Algorithm 5 Glaucoma screening

```

1: Input: OC segmentation optic_cup, OD segmentation optic_disc
2: Output: Glaucoma diagnosis diag
3: function GLAUCOMA_SCREENING(optic_cup, optic_disc)
4:   area_oc  $\leftarrow$  AREA_CALCULATION(optic_cup)
5:   area_od  $\leftarrow$  AREA_CALCULATION(optic_disc)
6:   CDR  $\leftarrow$   $\frac{\text{area\_oc}}{\text{area\_od}}$ 
7:   if CDR  $>$  0.63 then
8:     diag  $\leftarrow$  'Glaucomatous'
9:   else
10:    diag  $\leftarrow$  'Healthy'
11:   return diag
```

Using CDR calculation, glaucoma screening strategy is proposed in section 3.4.

3.4. Glaucoma screening

In this section, we present the approach for glaucoma screening and diagnosis, using the CDR feature. To achieve this required classification between healthy and glaucomatous subjects, many techniques are employed by existing glaucoma screening methods using different classifiers to assign the retinal images among their actual class (Singh et al., 2015b). One of the most popular glaucoma classifier is the Support Vector Machine (SVM), a supervised classification method which determinates a maximum-margin among the features to separate the classes (Maheshwari et al., 2017). An other well-known classification method for glaucoma screening is the k -Nearest Neighbor classifier (k -NN), a supervised method which associate each data to the predominant class of its k closest neighbors (with k a positive integer) (Bock et al., 2007). In these two supervised methods, several features need to be extracted in addition to the CDR to feed the supervised algorithm and improve the classification accuracy. Moreover, the choice of these features is challenging (Joshi et al., 2011).

CDR-based methods generally classify each retinal image using a binary classification method. It consists in the use of a soundly-chosen thresholding value T . Thus, using the computed CDR, a simple binary classification is operated. A

CDR value lower than the threshold value T agrees with a healthy subject, otherwise, it corresponds to a glaucomatous subject (Cheng et al., 2013; Singh et al., 2015b; Yin et al., 2011). In our work, this simple approach is used, providing more ease and less computational cost while trustworthiness in final glaucoma screening and diagnosis. Indeed, exploiting the CDR clinical factor involves more reliability and efficiency on the final classification, while avoiding the use of hardly-chosen image-based features for a greedy learning phase. Here, the challenge is to set a reliable threshold value, allowing to effectively separate healthy subjects from glaucomatous ones. To set up the accurate threshold value according to the CDR values within each healthy and glaucomatous class, we choose to compute the threshold value T depending on the mean \bar{m} and standard deviation σ of the obtained CDR values of each retinal images among healthy and glaucomatous classes in the annotated database (see Eq. 7).

$$\bar{m}_H + \sigma_H < T \leq \bar{m}_G - \sigma_G \quad (7)$$

where \bar{m}_H and \bar{m}_G are respectively the mean of healthy and glaucomatous computed CDR, and σ_H and σ_G are respectively the standard deviation of the healthy and glaucomatous computed CDR.

After proposing a complete methodology for glaucoma screening from fundus images, used materials and obtained experimental results of the proposed method are expressed in the following section.

4. Materials and Results

4.1. Materials

4.1.1. Databases

For OD detection, since the operation must be effective in many different clinical cases, the proposed method was evaluated on ten databases among the most popular public databases in retinal image study. In particular, they were developed to detect various ocular pathologies, test a diagnosis protocol or extract retinal structures, and were used in both medical or even non-medical contexts. VARIA (Ortega et al., 2009b,a) database contains 58 gray-scale images, used for the authentication of individuals via the vascular tree. DRIVE database (Staal et al., 2004) consists of 40 retinal images, and was developed for the segmentation of the retinal vascular tree. The STARE project (Hoover et al., 1998; Hoover and Goldbaum, 2003), mainly used to detect the OD, established a 81-images database with 31 healthy images and 50 pathological ones. MESSIDOR (Decencière et al., 2014) was created for diabetic retinopathy screening, with its 400 images. HRF database (High-Resolution Fundus) (Budai et al., 2013) with 45 images was established for diabetic retinopathy and glaucoma screening. ROC database (Niemeijer et al., 2010), created for micro-aneurysms detection linked to diabetic retinopathy, is composed of 50 images. DIARETDB0 (Kauppi et al., 2006) and DIARETDB1 (Kälviäinen and Uusitalo, 2007) were also developed for the detection of diabetic retinopathy. These databases include 130 and 89 retinal images respectively. Finally, the E-OPHTHA-EX and E-OPHTHA-MA databases (Decencière et al., 2013), respectively composed of 82 and 124 images, were mainly developed to detect different types of lesions caused by diabetic retinopathy (exudates, micro-aneurysms).

For OC and OD segmentation, and final glaucoma screening, the validation stage was conducted with the same database. The experiment was performed with the DRISHTI-GS1 database (Sivaswamy et al., 2014, 2015), which consists of 51 retinal color images, captured with a 30-degree FOV with a resolution of 2896 x 1944. For each captured image of the database, the ground-truth segmentation from four trained experts is provided for the OC and OD areas. The manual markings are computed in a soft map S , as the four segmentation results from each respective expert are superimposed in S . In our study, a preprocessing step was performed to obtain a three-expert majority consensus on the final ground-truth segmentation (Sivaswamy et al., 2015). This choice allows a good balance between a better unification of all clinical results, and a restricted but precise ground-truth area.

Moreover, for each retinal image from the database, the ground-truth glaucoma diagnosis by the four experts is also provided, with 18 healthy and 32 glaucomatous images. This final diagnosis by experts allows the validation of our glaucoma screening study and obtained results. Here, we use the group majority opinion with at least three out of four experts gives the final diagnosis, as the presence of a healthy or glaucomatous subject.

4.1.2. Evaluation metrics

For the experimental phase, we introduced several metrics to measure the performance of the proposed method. We exploit often-used metrics related to each stage of the algorithm (OD detection, OC and OD segmentation and glaucoma screening).

For OD detection, the performance is evaluated with the precision metric only. Here, a simple evaluation protocol is followed, as the OD detection point is considered correct if the point is inside the OD region, including its borders. Otherwise, the detection is considered wrong.

On the remainder of this experimental phase, the OC and OD segmentation and the glaucoma screening are assimilated to binary classification tasks. True positives (TP) gather all correctly-classified positive samples. Likewise, true negatives (TN) group all correctly-classified negative samples. Inversely, false positives (FP) gather the actual negative samples classified as positives, and false negatives (FN) gather the actual positive samples classified as negatives.

For the OC and OD segmentation, TP consist of all pixels correctly classified as part of the area, and TN gather all pixels correctly classified as non-part of the segmented area. Inversely, FP gather all pixels labeled as part of the segmented area, when they actually do not be part of the ground-truth manual marking. FN gather the pixels labeled as non-part of the segmented area, when they are actually part of the ground-truth manual marking.

To evaluate the segmentation step, we compute three metrics (Sivaswamy et al., 2015):

- Sensitivity, also called recall, denotes the proportion of correctly-classified positive pixels among the actual positive pixels:

$$Sen = \frac{TP}{TP + FN} \quad (8)$$

- The positive predictive value (PPV), also called precision, denotes the proportion of correctly-classified pixels among the labeled-positive pixels:

$$PPV = \frac{TP}{TP + FP} \quad (9)$$

- The F-score is a harmonic mean of sensitivity and PPV metrics:

$$F-score = 2 \cdot \frac{Sen \cdot PPV}{Sen + PPV} \quad (10)$$

For glaucoma screening and diagnosis, the same classification protocol is followed. TP define the subjects correctly diagnosed as glaucomatous. Likewise, TN gather the subjects correctly diagnosed as healthy. Inversely, FP represent the subjects diagnosed as glaucomatous, when they actually do not suffer from glaucoma. This type of error mainly causes a false alarm, with a potential unnecessary treatment. Even worse, the FN represent the subjects suffering from glaucoma, when they are detected as healthy by the glaucoma screening system. This second type of error causes more serious consequences, as the disease is not screened and a treatment at the earlier stage cannot be provided. The detection of the disease presence will occur at further stages, inducing a more expensive and inconvenient treatment. In this way, as an effective detection of potential glaucomatous subject is primordial, a non-healthy subject screening system at the cutting-edge is required. A maximum certainty on the positive labelling is expected.

In this direction, we compute the three metrics in Eq. (8), (9) and (10). For glaucoma screening, sensitivity denotes the proportion of correctly-classified glaucomatous subjects among all actual glaucomatous subjects. PPV denotes the proportion of subjects correctly labeled glaucomatous among the labeled-glucomatous ones. F-score is a harmonic mean of sensitivity and PPV metrics.

We also compute the three following metrics:

- Specificity (Spe) is the proportion of correctly-classified healthy subjects among all actual healthy subjects:

$$Spe = \frac{TN}{TN + FP} \quad (11)$$

- The negative predictive value (NPV) denotes the proportion of correctly-classified healthy subjects among the labeled-healthy ones:

$$NPV = \frac{TN}{TN + FN} \quad (12)$$

- Finally, the overall accuracy (Acc) is the proportion of correctly-classified subjects among all subjects (healthy or glaucomatous):

$$Acc = \frac{TP + TN}{TP + TN + FP + FN} \quad (13)$$

These metrics are used to evaluate the glaucoma screening method, by comparing each found diagnosis (healthy or glaucomatous) to the diagnosis from the trained specialists. Hence, in the medical context, these metrics can be interpreted by a ophthalmologist, to assess the usefulness of the system on the final diagnosis (Saunders et al., 2015). The results obtained on each evaluation metric are expressed in the following section.

4.2. Results

4.2.1. Computation efficiency

In this section, the time complexity of the proposed method for glaucoma screening is laid out. A summary can be found in Table 2. As noticed in the previous sections (see sections 1, 2), one of the main challenges in this work is to propose a computationally-efficient method for glaucoma screening and diagnosis. A further goal is to deploy computer-aided mobile systems, spreading the access to eye health.

We firstly proposed a new method for OD detection (see Algorithm 1). A prior rigorous study of the existing methods have been conducted. In the presented method, we exploited the brightness feature of the OD (see Algorithm 2) and a template matching technique (see Algorithm 3) to detect the OD even in the presence of lesions. The detection of the bright regions involves the computation of well-used computer vision algorithms such as Otsu's thresholding, Euclidean distance transform or the extraction of maximum values. Considering L different gray levels in the image, Otsu's thresholding involves in the worst case $\mathcal{O}(L^2)$ operations. Considering a retinal image I with a $n \times n$ size, the distance transform generates a $\mathcal{O}(n^2)$ complexity. Extracting max values in a n -length list involves a $\mathcal{O}(n)$ linear research in the worst case. Template matching involves the use of less costing algorithms, since the histogram calculation, the creation of the histogram templates and the matching using cross-correlation generate $\mathcal{O}(1)$ constant or $\mathcal{O}(n)$ linear time complexity. It is important to notice that template matching is applied on a few candidates and not along the whole image, inducing less operations. As a major advantage, the method avoids the extraction of the vascular tree to effectively detect the OD, often relying on $\mathcal{O}(n^3)$ cubic complexity algorithms (Ben Sayadia et al., 2018).

Secondly, for OC and OD segmentation (see Algorithm 4), a previous study of the existing methods conducts to propose an unsupervised segmentation method. Here, we used a K-means clustering approach, exploiting the intensity criterion to classify the pixels to each retinal area (see Algorithm 4, line 5). The main advantage of the K-means clustering is its quick convergence to the final clustering. Also, setting only two parameters (distance D , number of clusters K) allows quite ease. Despite the K-means clustering is a $\mathcal{O}(KDn^2)$ polynomial algorithm (with $n \times n$ the number of observations to classify) (Xu and Tian, 2015), it remains one of the computationally-efficient clustering approaches, in comparison with the fuzzy c-means clustering for instance (Ghosh and Dubey, 2013). In practice, with our small OD sub-images, K-means clustering is operated in real-time. A lot of works have improved the K-means clustering complexity, particularly by proposing an efficient initialization of the cluster centers (Celebi et al., 2013). Its practical convenience permits to converge toward a precise segmentation of the areas in an efficient manner.

To improve the segmentation accuracy, we have employed the circular Hough transform to fit on the boundaries (see Algorithm 4, line 16). Circular Hough transform have been extensively used over the decades for pattern recognition purpose (Mukhopadhyay and Chaudhuri, 2015). Recent studies have performed the Hough transform in real-time

(Weiss, 2008), and a lot of works have studied the Hough transform for an efficient implementation reducing its computational requirements (Hassanein et al., 2015; Soltany et al., 2011) with $\mathcal{O}(n^2)$ -complex algorithms. However, the complexity of the circular Hough transform can rapidly increase with the number of computed circles with different radius for each edge point of the image. Thus, to decrease the computational cost when computing the Hough transform, we restrict the search interval. For that we fix the radius R of the final circle in a well-defined interval. Here, we define the interval I_R as:

$$I_R = \left[\frac{R_{area}}{2}; \quad R_{area} + \frac{R_{area}}{2} \right] \quad (14)$$

where R_{area} corresponds respectively to the OC and OD radius approximations, as R_{OD} is defined in Eq. (2) and $R_{OC} \approx R_{OD}/2$. Hence, the circular Hough transform is performed with a few numbers of candidate circles.

Thirdly, for CDR calculation and glaucoma screening (see Algorithm 5), simple techniques such as the ratio calculation, and thresholding to classify healthy and glaucomatous subjects rely on $\mathcal{O}(1)$ constant time complexity. The prior calculation of the areas of the OC and OD regions relies on $\mathcal{O}(n^2)$ operations in the worst case. Finally, the full method for glaucoma screening relies on low-complex algorithms, with a $\mathcal{O}(n^2)$ order of n^2 total time complexity, in line with the expressed requirements for a prospective implementation on mobile devices.

Functions	Parameters	Time complexity
Otsu's thresholding	Number of gray levels L	$\mathcal{O}(L^2)$
Euclidean distance transform	Size of the image N	$\mathcal{O}(N^2)$
Extract values (max)	length of the list l	$\mathcal{O}(l)$
Template Matching	Number of histogram bins H	$\mathcal{O}(H^2)$
K-means clustering	Size of the crop m , number of clusters K , distance D	$\mathcal{O}(KDm^2)$
Circular Hough Transform	Size of the crop m	$\mathcal{O}(m^2)$

Table 2: Overview of the worst-case time complexity of the computed functions for glaucoma screening.

4.2.2. OD detection and ROI extraction

Fig. 10 presents a few qualitative results on OD detection, on both healthy (1) and pathological (2) retinal images. These results illustrate the ability to detect the OD, even in the presence of bright and spread lesions. In Fig. 11, a few examples of OD detection failures are illustrated. In (a), a gradual darkening around the OD is observed, inducing a challenging detection using its brightness feature. In (b) and (c), large bright regions within the retina have resulted to a missing of the OD area, since the lesions are significantly brighter than the OD. Also, applying the template matching to find the final OD location may induce a wrong identification in rarer extreme cases. The method for OD detection is applied on the different evaluation databases, and the obtained results are compared to the state-of-the-art methods. The proposed method achieves a 99.3% detection rate on the different images from the evaluation databases. In healthy retinal databases, where no bright lesions are apparent, such as VARIA, DRIVE,

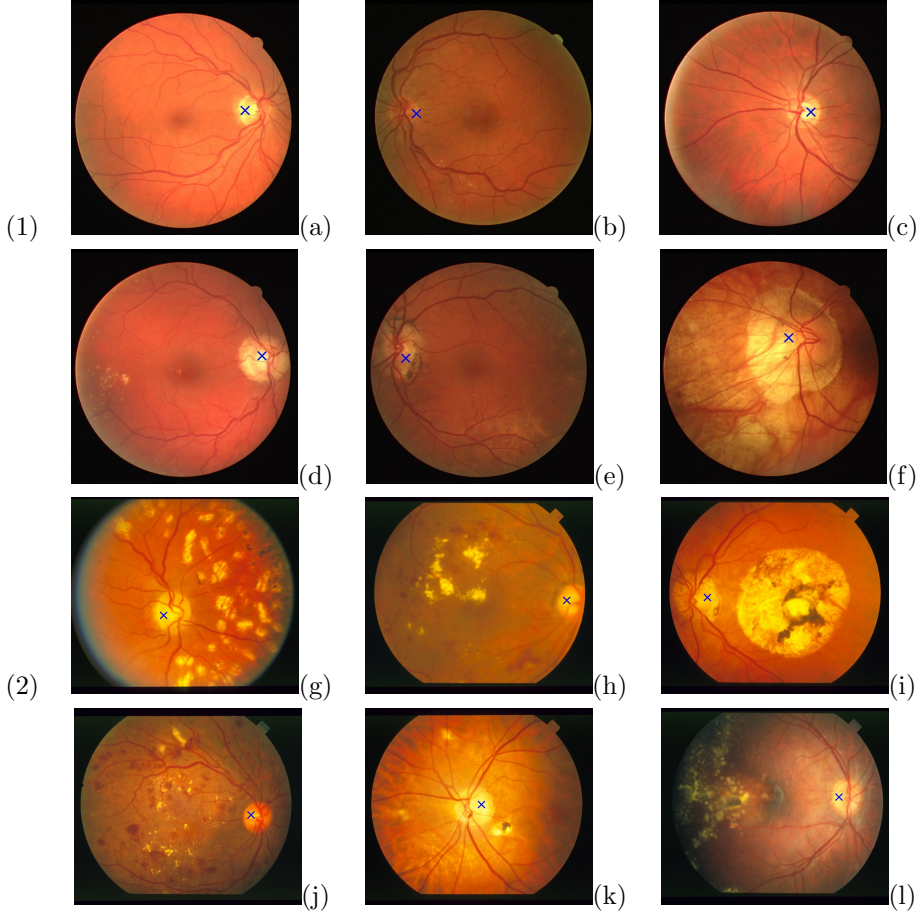


Figure 10: OD detection examples, in both healthy (1) and non-healthy (2) databases. The blue cross (\times) represents the found OD location point ((1) DRIVE database (six samples a, b, c, d, e, f), (2) STARE database (six samples g, h, i, j, k, l)).



Figure 11: OD detection failures, in both healthy (a) and non-healthy (b, c) cases. The blue cross (\times) represents the found OD location point.

ROC or HRF, a 100% detection is obtained. These results are equal or outperforms the state-of-the-art approaches for OD detection (Hashim et al., 2015; Mahfouz and Fahmy, 2010; Soares et al., 2016). In pathological cases, where bright lesions are apparent, excellent performance on OD detection are also reached. Performance rates between 97.78% and 99.49% are obtained on these non-healthy databases, such as STARE, MESSIDOR, DIARETDB0, DIARETDB1, E-OPHTHA-EX or E-OPHTHA-MA. These results show the algorithm capacity to effectively detect the OD even in the presence of bright lesions, often having the same brightness feature as the disc. Globally, the method tends to

outperform the state-of-the-art methods based on the brightness feature (Hashim et al., 2015; Pourreza-Shahri et al., 2014), and compete with the methods based on the vascular tree extraction (Mahfouz and Fahmy, 2010; Soares et al., 2016; Zhang and Zhao, 2016), while ensuring a low complexity cost.

4.2.3. OC and OD segmentation

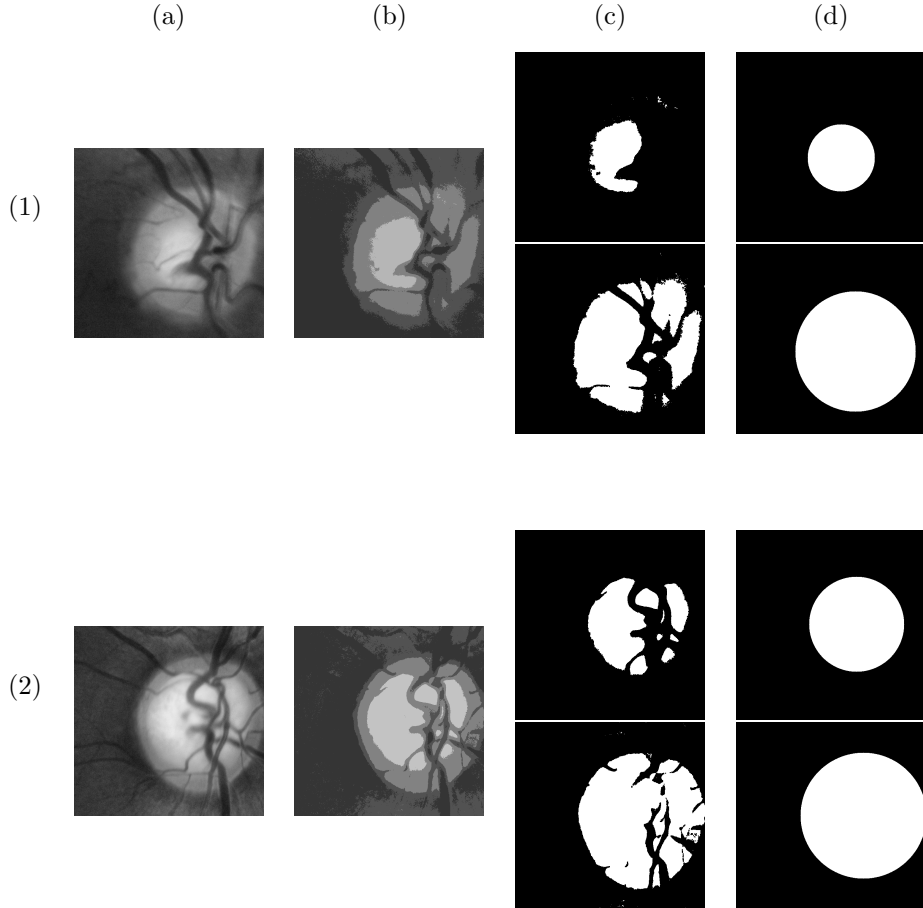


Figure 12: OC and OD segmentation examples, with healthy (1) and glaucomatous (2) images: (a) sub-image around the OD, (b) k-means clustering ($K=4$), (c) OC and OD extraction, (d) final segmentation with circular Hough transform.

Qualitative results for OC and OD segmentation are shown in Fig. 12, illustrating the results for healthy (1) and glaucomatous (2) images from DRISHTI-GS1 database. A different cupping within the ONH is apparent between the two different examples. For each OD sub-image (a), we compute the K-means algorithm (b). Then, the clusters corresponding to the OC and OD areas are extracted (c). Finally, the circular Hough transform allows to find the boundaries of each area (d).

The DRISHTI-GS1 database was used to evaluate the performance of our segmentation method. A relevant ground-truth segmentation by four trained experts is provided for the OC and OD areas of each retinal image, both important for the ONH assessment. Hence, DRISHTI-GS1 is a well-used and pertinent database to benchmark

different segmentation algorithms. The proposed method for OC and OD segmentation was evaluated with the three sensitivity, PPV and F-score metrics (see Eq. (8), (9) and (10)). These metrics reflect the ability of the method to effectively classify the pixels belonging to the respective areas (OC and OD).

For the sensitivity metric, 76.91% and 83.05% rates are obtained for the OC and OD areas respectively, testifying the encouraging performance of the segmentation method. For the PPV metric, excellent performance rates of 80.38% and 94.32% are respectively obtained for the OC and OD areas. For the F-score metric, top-notch performance rates are reached by our proposed method, with a 79% rate for the OC and a 91.45% rate for the OD.

We also compare our results with the state-of-the-art methods, validated on DRISHTI-GS1 database. This comparison is made with the F-score metric, quantifying the region overlap between the computed area and the ground truth (Sivaswamy et al., 2014). The F-score brings a relevant measurement of the segmentation performance (Joshi et al., 2011). According to the F-score value, our method outperforms the method in Wong et al. (2008) with 77.1% and compete with the method in Cheng et al. (2013) reaching a 78.9% rate. For the OD area, our method competes with the method in Wong et al. (2008) and Cheng et al. (2013), reaching 91.1% and 92.1% respectively. These results show the ability of the algorithm to effectively purchase and classify each pixel belonging to the areas.

Globally, we notice that decreased rates are obtained for the OC area. It is due to the arduous task on effectively detect the borders, when the OC have not-well defined boundaries. It is the same case for the existing state-of-the-art methods. Anyway, our segmentation stage achieves good performance and compete over the state-of-the-art methods, while using less complex algorithms. This precise segmentation allows a good approximation of the area-based CDR value for glaucoma screening.

4.2.4. Glaucoma screening

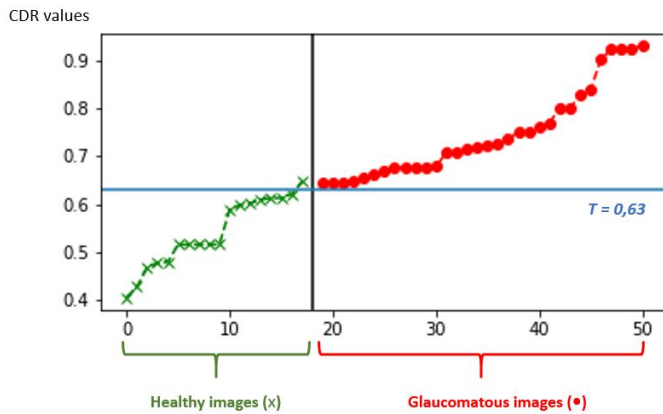


Figure 13: CDR value for each retinal image, from healthy (green) class and glaucomatous (red) class (along x-axis: fifty annotated images from DRISHTI-GS1, along y-axis: CDR values (between 0 and 1)). The threshold value $T = 0.63$ is plotted in blue line along y-axis.

Healthy class		Glaucomatous class	
Mean \bar{m}_H	Standard deviation σ_H	Mean \bar{m}_G	Standard deviation σ_G
0.541	0.07	0.74	0.09

Table 3: CDR mean and standard deviation values for healthy and glaucomatous classes.

Fig. 13 presents a graph with the computed CDR_{area} value for each image from the annotated part of DRISHTI-GS1 database. Here, two distinct colors are apparent, according to the actual class of each retinal image: healthy

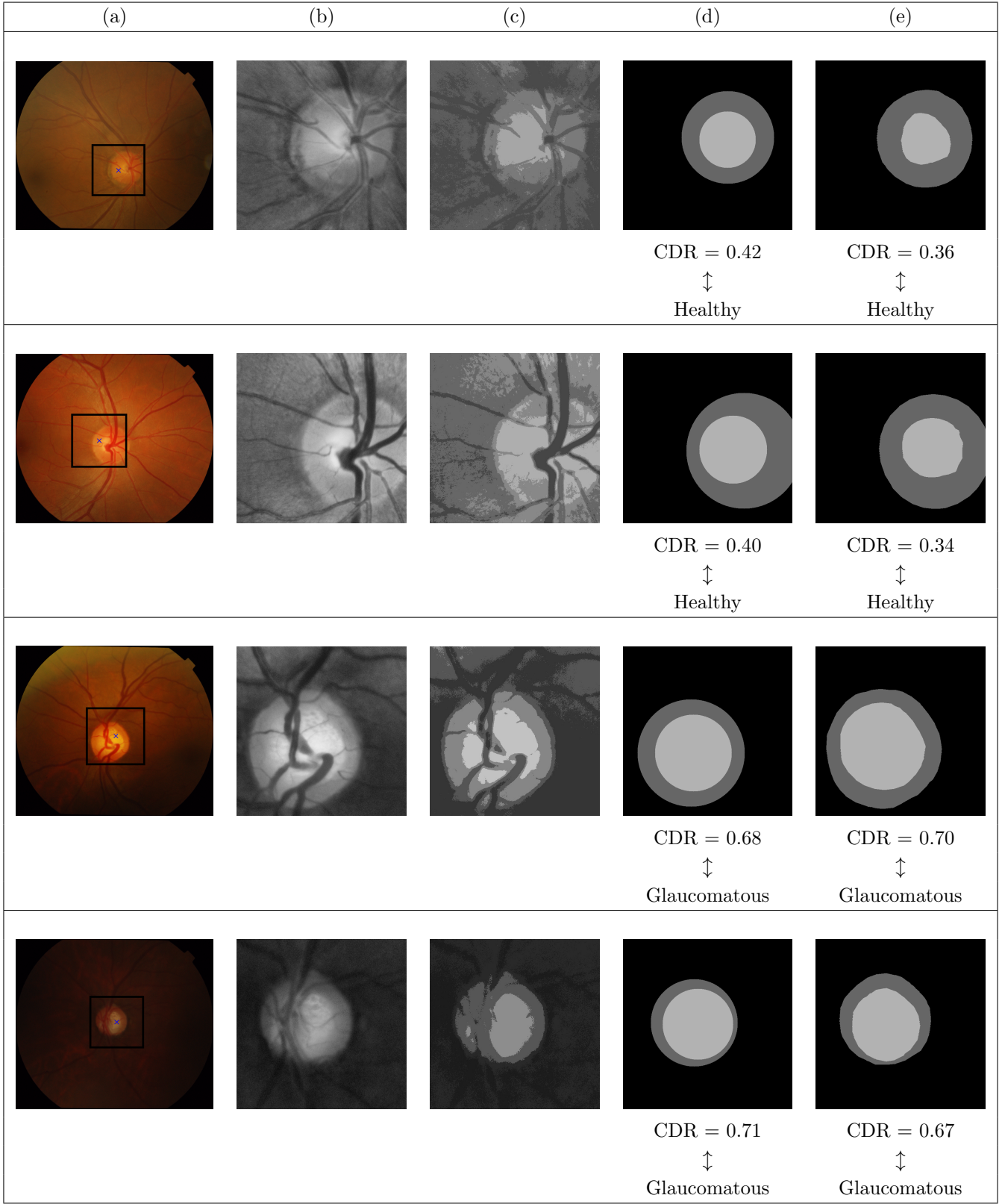


Figure 14: Qualitative results of the applied approach for glaucoma screening and diagnosis: (a) original retinal image, with OD location point (b) ROI extraction: sub-image around the OD, (c) k-means clustering ($K=4$), (d) joint OC-OD segmentation with CDR result and final diagnosis, (e) ground-truth joint OC-OD segmentation with CDR result and final diagnosis.

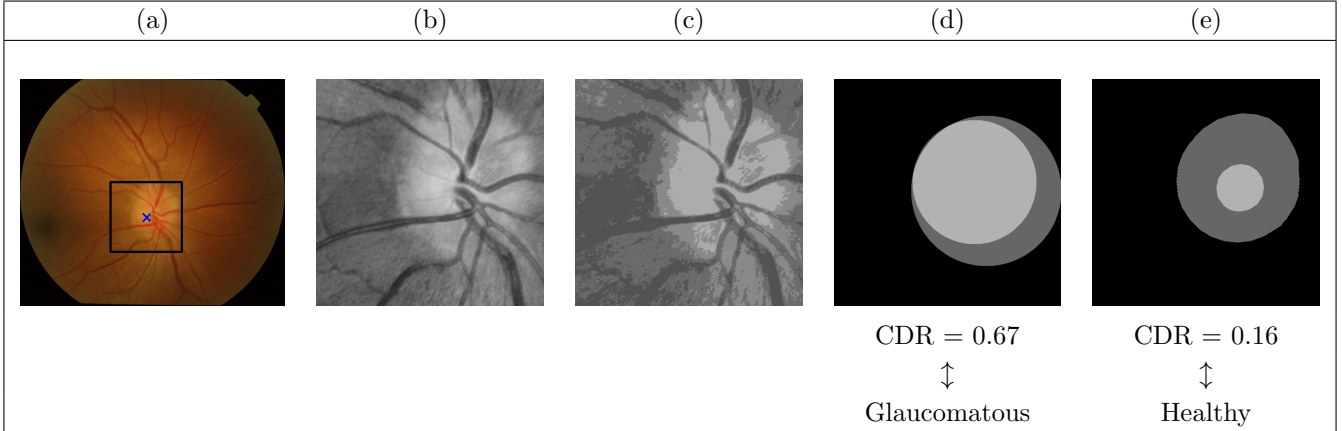


Figure 15: Glaucoma screening failure: (a) original retinal image, with OD location point (b) ROI extraction: sub-image around the OD, (c) k-means clustering ($K=4$), (d) joint OC-OD segmentation with CDR result and final diagnosis, (e) ground-truth joint OC-OD segmentation with CDR result and final diagnosis. The resulting segmentation leads to overestimated regions, and the CDR computation conducts to a false positive prediction.

images are represented in green color, when glaucomatous images are plotted in red color. Hence, CDR calculation finally leads to glaucoma screening and diagnosis. As explained in section 3.4 with the Eq. (7), the threshold value T is defined with the mean and standard deviation of each healthy and glaucomatous classes. Table 3 presents the CDR mean value, as well as the standard deviation within each class. According to these values, the obtained threshold value $T = 0.63$ is also plotted in the graph, along the y-axis (see Fig. 13). This threshold value T is used to classify each image to its class (healthy or glaucomatous).

Fig. 14 shows some examples of the obtained results by our proposed method for glaucoma screening. Starting from each input image in the evaluation database, the OD is located (see Fig 14 (b)) then extracted using the method for OD detection described in section 3.1. Fig 14 (c) shows this procedure. For the entire DRISHTI-GS1 database, an OD detection rate of 100% is obtained, ensuring an efficient glaucoma screening process. Since the evaluation database is composed of healthy or glaucomatous images only, no bright lesions linked to other ocular diseases are apparent. However, the robust OD detection method is useful with eventual bright lesions, going with subjects suffering from other ocular diseases. Then, our OC and OD segmentation method is performed using the approach described in section 3.2. In Fig. 14 (d), the segmentation result is shown for OC and OD areas. Also, the ground-truth segmentation provided by the trained experts is exposed in Fig. 14 (e). Afterwards, the area-based CDR is computed, using the segmentation result. With the threshold value T and the computed CDR_{area} value for each retinal image, the binary classification is applied. In Fig. 15, a failure in glaucoma screening is illustrated. Here, from the extracted sub-image around the OD (a), the OC and OD regions are segmented using the proposed method (b). Then, CDR computation leads to glaucoma screening using the defined threshold value. Here, since the boundaries of the regions of interest are difficult to define, overestimated OC and even OD regions are extracted. Hence, the computed segmentation affects the final result in glaucoma assessment, as the patient is wrongly diagnosed as suffering from glaucoma.

Metric	Guerre et al. (2014)	Wong et al. (2008)	Cheng et al. (2013)	Ayub et al. (2016)	Joshi et al. (2011)	Singh et al. (2015a)	Proposed Method
Acc	89	89.4	90.2	92	92.1	95	98
Sen	93	86.4	87.4	93	89.8	100	100
Spe	85	92.0	92.5	88	94.0	91	94.4
PPV	88	-	-	-	-	89	96.9
NPV	93	-	-	-	-	100	100
F-Score	90	-	-	-	-	94	98.4

Table 4: Obtained performance rates for glaucoma screening and diagnosis, in comparison with state-of-the art methods (%).

Following this, Table 4 exhibits the performance results, in comparison with some of the existing state-of-the-art methods for glaucoma screening.

The proposed method achieves excellent results and improves the state-of-the-art methods on the performed metrics. An accuracy rate of 98% on all the images is achieved, greater than the presented methods with performance rates between 89% and 95%. According to the accuracy rate and in accordance with the medical context, 98 subjects are well-diagnosed among 100 subjects with our proposed glaucoma screening method. For the sensitivity metric, a 100% rate is obtained, equal to the method in Singh et al. (2015a) and outperforming the other presented methods. That means that among 100 subjects actually suffering from glaucoma, the 100 subjects are detected as glaucomatous by the glaucoma screening system. This result strengthens the ability to effectively detect the glaucoma presence, in accordance with the motivations mentioned in section 4.1.2. For specificity, the proposed method reaches an excellent rate of 94.4%, superior to the presented methods. Among 100 healthy subjects, more than 94 subjects are effectively considered as healthy by our glaucoma screening method. Less than 6 healthy subjects are considered as suffering from glaucoma, representing a false but non-serious alarm. For the PPV metric, our proposed method for glaucoma diagnosis obtains a 96.9% rate, at least 7.9% higher than the other approaches. This value highlights the system quality to properly classify an actual glaucomatous image, among all the images labeled as being affected by the disease. Also, for the NPV metric associated to the healthy class, a rate of 100% equal to Singh et al. (2015a) method is reached, overriding the method in Guerre et al. (2014). Finally, the F-score rate reaches the highest value with 98.4%. In accordance with the medical context in this work, this metric value highlights the system effectiveness on glaucoma labelling, while having well ability to find all actual glaucomatous images in the experimental sample.

4.2.5. Computation time

We implemented the proposed method for glaucoma screening on a Python environment with Anaconda, using an 3.3 GHz Intel Xeon CPU system with 8Gb of RAM. The computation time was evaluated in terms of average runtime for the images in DRISHTI-GS1 database. The prior and offline template creation is done in 2.56 s, allowing to construct the OD model for further OD detection. According to the online method for glaucoma screening, the first OD detection method (detection of bright regions, template matching) requires a computation time of 8.31 s per image. For OC and OD segmentation, the K-means clustering algorithm requires a computation time of 0.9 s. For the Hough transform, finding the boundary circle is made in an average time of 2.08 s. CDR calculation and glaucoma screening are almost instantaneous. Finally, the full-method is computed in 11 s, showing off short computation time without any parallel optimization. This is in accordance with one of the purposes of this work formulated previously, as further implementation on portable platforms is intended.

5. Discussion

Several contributions are made in this study, to reveal an effective algorithm for glaucoma screening. Throughout the proposed method, a particular attention was assigned to the computational aspect, to provide an easy-to-perform and computationally-efficient method. Finally, we have obtained a final 98% accuracy rate on glaucoma screening.

First, the prior OD detection tends to propose an efficient way to detect the OD area, among the eventual presence of bright lesions in pathological cases. These bright lesions, linked to ocular diseases such as diabetic retinopathy, are not related to the glaucoma case. However, it is mandatory to efficiently conduct glaucoma screening, even with a subject suffering from an ocular disease inducing the apparition of these bright lesions. A preprocessing step, followed by the combination of the detection of bright regions and a template matching allows to effectively detect the OD, in a computationally-efficient way. This stage of the method offers a robust location of the area of interest, without extracting the retinal vessels inducing a more important complexity. Since the prior OD detection can be quite sensitive in pathological cases, and need to be effective to lead to glaucoma screening, it have been tested on ten relevant databases in this field, showing an excellent performance on both healthy and non-healthy images. One limitation here is the decreased ability to detect the OD in critical cases, where the OD appears in darker images, with uneven illumination or weak contrast. However, we consider that the OD seems to be brighter than the retinal background, and the method was designed with this assumption.

Second, a new method for joint OC-OD segmentation have been proposed. The main challenge was to perform an accurate and inexpensive segmentation of the areas. Here, an unsupervised classification method is firstly employed, using the texture-based information and assigning each pixel within a retinal component. From there, to improve the segmentation accuracy, a boundary fitting algorithm based on the circular Hough transform is performed. The main advantage of the proposed segmentation method is its accuracy on finding each pixel belonging to the desired areas. However, the method relies on the intensity feature, which can be not obvious in extreme cases. Nevertheless, applying our method from 2-D retinal images by combining intensity information and the boundary fitting allows to converge toward a precise approximation of the areas.

Third, the clinical CDR feature is used to assess the ONH structural changes, and detect the eventual presence of the glaucoma disease. The CDR have been extensively used for this purpose, because of its clinical reliability. Here, we computed the area-based CDR, providing a 2-D evaluation of the cupping within the ONH. Then, we applied a thresholding on the CDR value to classify each retinal image belonging to the healthy class or the glaucomatous class. Following clinical studies and existing methods for this purpose, the thresholding value T have been chosen regarding to the within-class variance. In our specific study, a fixed value T is defined, to finally assign each retinal image among a class and give a diagnosis. Nevertheless, it can be useful to exploit the obtained mean and standard deviation values within each class, and exploit it in a different manner, such as proposing a more-effective way to assess glaucoma early or even grading the spreading of the glaucoma disease. In our study, a specific value T have been fixed, and we focused on comparing each assignment to the ground-truth result, in order to evaluate the effectiveness on final glaucoma screening. Anyway, by performing the prior OD detection and OC-OD segmentation, the clinical CDR feature allows to detect and identify any potential subject suffering from an early occurring glaucoma.

In this work, a fully-automated method was proposed, using traditional approaches with well-known computer vision algorithms. The new emerging deep learning approaches provide an end-to-end classification, automatically extracting features from the image through a prior learning with a certain amount of labelled data. Nowadays, these new algorithms are extensively used in medical image analysis, bringing an invaluable help for the screening of ocular diseases for instance (Gulshan et al., 2016). These cutting-edge algorithms have been exploited by recent state-of-the-art methods for glaucoma screening, unveiling interesting results in the assessment of the disease (Norouzifard et al., 2018; Zilly et al., 2017).

6. Conclusion and perspectives

In this paper, a new approach for glaucoma screening and diagnosis was proposed. Using the CDR clinical feature, the method automatically detects the presence of glaucoma, from 2-D retinal images. We focused on the computational aspect throughout the proposition of the algorithm. A four-stages strategy was followed: robust OD detection in healthy and pathological cases, joint OC-OD segmentation framework using texture-based and model-based criteria, area-based CDR calculation, and final glaucoma classification between healthy and non-healthy subjects. Using the presented evaluation databases and performance metrics, the proposed glaucoma screening approach reached a 98% accuracy rate on final screening, outperforming the state-of-the-art methods for this purpose. Since the approach offers excellent performance rates, it can be employed on a large-scale screening program of the glaucoma disease, and be incorporated in computer-aided diagnosis systems for ophthalmologists.

At the present time, we are working on the implementation of the proposed method for glaucoma screening on smartphone-captured fundus images. Starting from the retinal image acquisition with a dedicated device, the aim is to assess glaucoma on portable platforms as an app, from the OD detection to the final diagnosis between healthy or potentially suffering from glaucoma. Hence, the system can be employed by medical specialists, to ensure their final screening of the disease.

In future work, we propose to explore deep learning algorithms to deliver improved, cutting-edge systems for early glaucoma screening and diagnosis. We aim to provide a precise assessment of the retinal structures, to help ophthalmologists and clinicians reinforce their diagnosis and monitor the potential presence of the disease during time.

References

- Abràmoff, M. D., Garvin, M. K., and Sonka, M. (2010). Retinal imaging and image analysis. *IEEE reviews in biomedical engineering*, 3:169–208.
- Access Economics (2008). Tunnel vision: the economic impact of primary open angle glaucoma.
- Achanta, R., Shaji, A., Smith, K., Lucchi, A., Fua, P., and Süstrunk, S. (2012). Slic superpixels compared to state-of-the-art superpixel methods. *IEEE transactions on pattern analysis and machine intelligence*, 34(11):2274–2282.
- Aquino, A., Gegúndez-Arias, M. E., and Marín, D. (2010). Detecting the optic disc boundary in digital fundus images using morphological, edge detection, and feature extraction techniques. *IEEE transactions on medical imaging*, 29(11):1860–1869.
- Ayub, J., Ahmad, J., Muhammad, J., Aziz, L., Ayub, S., Akram, U., and Basit, I. (2016). Glaucoma detection through optic disc and cup segmentation using k-mean clustering. In *2016 International Conference on Computing, Electronic and Electrical Engineering (ICE Cube)*, pages 143–147. IEEE.
- Ben Sayadia, S., Elloumi, Y., Akil, M., and Bedoui, M. H. (2018). Computational efficiency of optic disk detection on fundus image: a survey. In *Society of Photo-Optical Instrumentation Engineers (SPIE) Conference Series*, volume 10670.
- Blanckenberg, M., Worst, C., and Scheffer, C. (2011). Development of a mobile phone based ophthalmoscope for telemedicine. In *2011 Annual International Conference of the IEEE Engineering in Medicine and Biology Society*, pages 5236–5239. IEEE.
- Bock, R., Meier, J., Michelson, G., Nyùl, L., and Hornegger, J. (2007). Classifying glaucoma with image-based features from fundus photographs. *Pattern Recognition*, page 355–364.
- Bock, R., Meier, J., Nyùl, L. G., Hornegger, J., and Michelson, G. (2010). Glaucoma risk index: automated glaucoma detection from color fundus images. *Medical image analysis*, 14(3):471–481.
- Bourne, R. R. (2007). Papille optique et glaucome. *Revue de Santé Oculaire Communautaire*, 4(3):8–9.
- Bourne, R. R., Flaxman, S. R., Braithwaite, T., Cicinelli, M. V., Das, A., Jonas, J. B., Keeffe, J., Kempen, J. H., Leasher, J., Limburg, H., et al. (2017). Magnitude, temporal trends, and projections of the global prevalence of blindness and distance and near vision impairment: a systematic review and meta-analysis. *The Lancet Global Health*, 5(9):e888–e897.

- Bourouis, A., Feham, M., Hossain, M. A., and Zhang, L. (2014). An intelligent mobile based decision support system for retinal disease diagnosis. *Decision Support Systems*, 59:341–350.
- Budai, A., Bock, R., Maier, A., Hornegger, J., and Michelson, G. (2013). Robust vessel segmentation in fundus images. *International journal of biomedical imaging*, 2013.
- Celebi, M. E., Kingravi, H. A., and Vela, P. A. (2013). A comparative study of efficient initialization methods for the k-means clustering algorithm. *Expert systems with applications*, 40(1):200–210.
- Chakravarty, A. and Sivaswamy, J. (2017). Joint optic disc and cup boundary extraction from monocular fundus images. *Computer methods and programs in biomedicine*, 147:51–61.
- Cheng, J., Liu, J., Xu, Y., Yin, F., Wong, D. W. K., Tan, N.-M., Tao, D., Cheng, C.-Y., Aung, T., and Wong, T. Y. (2013). Superpixel classification based optic disc and optic cup segmentation for glaucoma screening. *IEEE transactions on Medical Imaging*, 32(6):1019–1032.
- Chrástek, R., Wolf, M., Donath, K., Niemann, H., Paulus, D., Hothorn, T., Lausen, B., Lämmer, R., Mardin, C. Y., and Michelson, G. (2005). Automated segmentation of the optic nerve head for diagnosis of glaucoma. *Medical Image Analysis*, 9(4):297–314.
- Costagliola, C., Dell’Omo, R., Romano, M., Zeppa, L., and Parmeggiani, F. (2009a). Pharmacotherapy of intraocular pressure: part ii. parasympathomimetic, sympathomimetic and sympatholytics. *Expert Opin Pharmacother*, 10(17):2859–2870.
- Costagliola, C., Dell’Omo, R., Romano, M. R., Rinaldi, M., Zeppa, L., and Parmeggiani, F. (2009b). Pharmacotherapy of intraocular pressure: part i. parasympathomimetic, sympathomimetic and sympatholytics. *Expert opinion on Pharmacotherapy*, 10(16):2663–2677.
- Decencière, E., Cazuguel, G., Zhang, X., Thibault, G., Klein, J.-C., Meyer, F., Marcotegui, B., Quellec, G., Lamard, M., Danno, R., et al. (2013). Teleophta: Machine learning and image processing methods for teleophthalmology. *Irbm*, 34(2):196–203.
- Decencière, E., Zhang, X., Cazuguel, G., Lay, B., Cochener, B., Trone, C., Gain, P., Ordonez, R., Massin, P., Erginay, A., et al. (2014). Feedback on a publicly distributed image database: the messidor database. *Image Analysis & Stereology*, 33(3):231–234.
- Dehghani, A., Moghaddam, H. A., and Moin, M.-S. (2012). Optic disc localization in retinal images using histogram matching. *EURASIP Journal on Image and Video Processing*, 2012(1):19.
- Elloumi, Y., Akil, M., and Kehtarnavaz, N. (2018). A mobile computer aided system for optic nerve head detection. *Computer methods and programs in biomedicine*, 162:139–148.

- Fingeret, M., Medeiros, F. A., Susanna Jr, R., and Weinreb, R. N. (2005). Five rules to evaluate the optic disc and retinal nerve fiber layer for glaucoma. *Optometry-Journal of the American Optometric Association*, 76(11):661–668.
- Flaxman, S. R., Bourne, R. R., Resnikoff, S., Ackland, P., Braithwaite, T., Cincinelli, M. V., Das, A., Jonas, J. B., Keeffe, J., Kempen, J. H., et al. (2017). Global causes of blindness and distance vision impairment 1990–2020: a systematic review and meta-analysis. *The Lancet Global Health*, 5(12):e1221–e1234.
- Foracchia, M., Grisan, E., and Ruggeri, A. (2004). Detection of optic disc in retinal images by means of a geometrical model of vessel structure. *IEEE transactions on medical imaging*, 23(10):1189–1195.
- Foster, A. and Johnson, G. J. (1990). Magnitude and causes of blindness in the developing world. *International ophthalmology*, 14(3):135–140.
- Foster, P. J., Buhrmann, R., Quigley, H. A., and Johnson, G. J. (2002). The definition and classification of glaucoma in prevalence surveys. *British journal of ophthalmology*, 86(2):238–242.
- Ghosh, S. and Dubey, S. K. (2013). Comparative analysis of k-means and fuzzy c-means algorithms. *International Journal of Advanced Computer Science and Applications*, 4(4).
- Giraddi, S., Pujari, J., and Hiremath, P. (2017). Optic disc detection using geometric properties and gvf snake. In *2017 1st International Conference on Intelligent Systems and Information Management (ICISIM)*, pages 141–146. IEEE.
- Guerre, A., Martinez-del Rincon, J., Miller, P., and Azuara-Blanco, A. (2014). Automatic analysis of digital retinal images for glaucoma detection. *Irish Machine Vision and Image Processing Conference*.
- Gulshan, V., Peng, L., Coram, M., Stumpe, M. C., Wu, D., Narayanaswamy, A., Venugopalan, S., Widner, K., Madams, T., Cuadros, J., et al. (2016). Development and validation of a deep learning algorithm for detection of diabetic retinopathy in retinal fundus photographs. *Jama*, 316(22):2402–2410.
- Hashim, F., Salem, N., and Seddik, A. F. (2015). Optic disc boundary detection from digital fundus images. *Journal of Medical Imaging and Health Informatics*, 5(1):50–56.
- Hassanein, A. S., Mohammad, S., Sameer, M., and Ragab, M. E. (2015). A survey on hough transform, theory, techniques and applications. *arXiv preprint arXiv:1502.02160*.
- Hoover, A. and Goldbaum, M. (2003). Locating the optic nerve in a retinal image using the fuzzy convergence of the blood vessels. *IEEE transactions on medical imaging*, 22(8):951–958.
- Hoover, A., Kouznetsova, V., and Goldbaum, M. (1998). Locating blood vessels in retinal images by piece-wise threshold probing of a matched filter response. In *Proceedings of the AMIA Symposium*, page 931. American Medical Informatics Association.

- Hu, M., Zhu, C., Li, X., and Xu, Y. (2017). Optic cup segmentation from fundus images for glaucoma diagnosis. *Bioengineered*, 8(1):21–28.
- Inoue, N., Yanashima, K., Magatani, K., and Kurihara, T. (2006). Development of a simple diagnostic method for the glaucoma using ocular fundus pictures. In *2005 IEEE Engineering in Medicine and Biology 27th Annual Conference*, pages 3355–3358. IEEE.
- Jonas, J. B., Fernández, M. C., and Naumann, G. O. H. (1992). Glaucomatous Parapapillary Atrophy: Occurrence and Correlations. *JAMA Ophthalmology*, 110(2):214–222.
- Joshi, G. D., Sivaswamy, J., and Krishnadas, S. (2011). Optic disk and cup segmentation from monocular color retinal images for glaucoma assessment. *IEEE transactions on medical imaging*, 30(6):1192–1205.
- Kälviäinen, R. and Uusitalo, H. (2007). Diaretldb1 diabetic retinopathy database and evaluation protocol. In *Medical Image Understanding and Analysis*, volume 2007, page 61. Citeseer.
- Kauppi, T., Kalesnykiene, V., Kamarainen, J.-K., Lensu, L., Sorri, I., Uusitalo, H., Kälviäinen, H., and Pietilä, J. (2006). Diaretldb0: Evaluation database and methodology for diabetic retinopathy algorithms. *Machine Vision and Pattern Recognition Research Group, Lappeenranta University of Technology, Finland*, 73.
- Kingman, S. (2004). Glaucoma is second leading cause of blindness globally. *Bulletin of the World Health Organization*, 82:887–888.
- Kodinariya, T. M. and Prashant, R. M. (2014). Survey on exiting method for selecting initial centroids in k-means clustering. *International Journal of Engineering Development and Research*.
- Lim, T.-C., Chattopadhyay, S., and Acharya, U. R. (2012). A survey and comparative study on the instruments for glaucoma detection. *Medical engineering & physics*, 34(2):129–139.
- Liu, J., Wong, D., Lim, J., Li, H., Tan, N., Zhang, Z., Wong, T., and Lavanya, R. (2009). Argali: an automatic cup-to-disc ratio measurement system for glaucoma analysis using level-set image processing. In *13th International Conference on Biomedical Engineering*, pages 559–562. Springer.
- MacQueen, J. et al. (1967). Some methods for classification and analysis of multivariate observations. In *Proceedings of the fifth Berkeley symposium on mathematical statistics and probability*, volume 1, pages 281–297. Oakland, CA, USA.
- Maheshwari, S., Pachori, R. B., Kanhangad, V., Bhandary, S. V., and Acharya, U. R. (2017). Iterative variational mode decomposition based automated detection of glaucoma using fundus images. *Computers in biology and medicine*, 88:142–149.
- Mahfouz, A. E. and Fahmy, A. S. (2010). Fast localization of the optic disc using projection of image features. *IEEE Transactions on Image Processing*, 19(12):3285–3289.

- Maldhure, P. N. and Dixit, V. (2015). Glaucoma detection using optic cup and optic disc segmentation. *International Journal of Engineering Trends and Technology (IJETT)*, 20(2):52–55.
- Medeiros, F. A., Zangwill, L. M., Bowd, C., Vessani, R. M., Susanna Jr, R., and Weinreb, R. N. (2005). Evaluation of retinal nerve fiber layer, optic nerve head, and macular thickness measurements for glaucoma detection using optical coherence tomography. *American journal of ophthalmology*, 139(1):44–55.
- Mukhopadhyay, P. and Chaudhuri, B. B. (2015). A survey of hough transform. *Pattern Recognition*, 48(3):993–1010.
- Niemeijer, M., Van Ginneken, B., Cree, M. J., Mizutani, A., Quellec, G., Sánchez, C. I., Zhang, B., Hornero, R., Lamard, M., Muramatsu, C., et al. (2010). Retinopathy online challenge: automatic detection of microaneurysms in digital color fundus photographs. *IEEE transactions on medical imaging*, 29(1):185–195.
- Norouzifard, M., Nemati, A., GholamHosseini, H., Klette, R., Nouri-Mahdavi, K., and Yousefi, S. (2018). Automated glaucoma diagnosis using deep and transfer learning: Proposal of a system for clinical testing. In *2018 International Conference on Image and Vision Computing New Zealand (IVCNZ)*, pages 1–6. IEEE.
- Nugraha, G. S. and Soesanti, I. (2016). Segmentation of the optic disc and optic cup using histogram feature-based adaptive threshold for cup to disk ratio. In *MATEC Web of Conferences*, volume 75, page 05003. EDP Sciences.
- Ortega, M., Penedo, M. G., Rouco, J., Barreira, N., and Carreira, M. J. (2009a). Personal verification based on extraction and characterisation of retinal feature points. *Journal of Visual Languages & Computing*, 20(2):80–90.
- Ortega, M., Penedo, M. G., Rouco, J., Barreira, N., and Carreira, M. J. (2009b). Retinal verification using a feature points-based biometric pattern. *EURASIP Journal on Advances in Signal Processing*, 2009:2.
- Osareh, A., Mirmehdi, M., Thomas, B., and Markham, R. (2003). Automated identification of diabetic retinal exudates in digital colour images. *British Journal of Ophthalmology*, 87(10):1220–1223.
- Pascolini, D. and Mariotti, S. P. (2012). Global estimates of visual impairment: 2010. *British Journal of Ophthalmology*, 96(5):614–618.
- Pedersen, S. J. K. (2007). Circular hough transform. *Aalborg University, Vision, Graphics, and Interactive Systems*, 123(6).
- Pizer, S. M., Amburn, E. P., Austin, J. D., Cromartie, R., Geselowitz, A., Greer, T., ter Haar Romeny, B., Zimmerman, J. B., and Zuiderveld, K. (1987). Adaptive histogram equalization and its variations. *Computer vision, graphics, and image processing*, 39(3):355–368.
- Pourreza-Shahri, R., Tavakoli, M., and Kehtarnavaz, N. (2014). Computationally efficient optic nerve head detection in retinal fundus images. *Biomedical Signal Processing and Control*, 11:63–73.
- Priyadharsini, R., Beulah, A., and Sharmila, T. S. (2018). Optic disc and cup segmentation in fundus retinal images using feature detection and morphological techniques. *CURRENT SCIENCE*, 115(4):748.

- Quigley, H. A. and Broman, A. T. (2006). The number of people with glaucoma worldwide in 2010 and 2020. *British journal of ophthalmology*, 90(3):262–267.
- Radon, J. (1986). On the determination of functions from their integral values along certain manifolds. *IEEE transactions on medical imaging*, 5(4):170–176.
- Rahebi, J. and Hardalaç, F. (2016). A new approach to optic disc detection in human retinal images using the firefly algorithm. *Medical & biological engineering & computing*, 54(2-3):453–461.
- Saunders, L. J., Zhu, H., Bunce, C., Doré, C. J., Freemantle, N., Crabb, D. P., et al. (2015). Ophthalmic statistics note 5: diagnostic tests—sensitivity and specificity. *British Journal of Ophthalmology*, 99(9):1168–1170.
- Shen, S. Y., Wong, T. Y., Foster, P. J., Loo, J.-L., Rosman, M., Loon, S.-C., Wong, W. L., Saw, S.-M., and Aung, T. (2008). The prevalence and types of glaucoma in malay people: the singapore malay eye study. *Investigative ophthalmology & visual science*, 49(9):3846–3851.
- Singh, M., Singh, M., and Jiwanpreet, K. (2015a). Glaucoma screening using compensated cup-to-disk ratio value. *International Journal of Computer Science & Communication*, 6(2):83–91.
- Singh, M., Singh, M., and JiwanpreetKaurVirk (2015b). Glaucoma detection techniques: A review. *Computer Science and Electronics Journals*, 6(2):66–76.
- Sivaswamy, J., Krishnadas, S., Chakravarty, A., Joshi, G., Tabish, A. S., et al. (2015). A comprehensive retinal image dataset for the assessment of glaucoma from the optic nerve head analysis. *JSM Biomedical Imaging Data Papers*, 2(1):1004.
- Sivaswamy, J., Krishnadas, S., Joshi, G. D., Jain, M., and Tabish, A. U. S. (2014). Drishti-gs: Retinal image dataset for optic nerve head (ohn) segmentation. In *2014 IEEE 11th International Symposium on Biomedical Imaging (ISBI)*, pages 53–56. IEEE.
- Soares, I., Castelo-Branco, M., and Pinheiro, A. M. (2016). Optic disc localization in retinal images based on cumulative sum fields. *IEEE journal of biomedical and health informatics*, 20(2):574–585.
- Soltany, M., Zadeh, S. T., and Pourreza, H.-R. (2011). Fast and accurate pupil positioning algorithm using circular hough transform and gray projection. In *International Conference on Computer Communication and Management*.
- Staal, J., Abràmoff, M. D., Niemeijer, M., Viergever, M. A., and Van Ginneken, B. (2004). Ridge-based vessel segmentation in color images of the retina. *IEEE transactions on medical imaging*, 23(4):501–509.
- Stapor, K., Świtonski, A., Chrastek, R., and Michelson, G. (2004). Segmentation of fundus eye images using methods of mathematical morphology for glaucoma diagnosis. In *International Conference on Computational Science*, pages 41–48. Springer.

- Thakkar, K., Chauhan, K., Sudhalkar, A., Gulati, R., and Ophthalmologist, M. (2017). Detection of glaucoma from retinal fundus images by analysing isn't measurement and features of optic cup and blood vessels. *Int. J. Eng. Technol. Sci. IJETSR*, 4(7):2394–3386.
- Tham, Y.-C., Li, X., Wong, T. Y., Quigley, H. A., Aung, T., and Cheng, C.-Y. (2014). Global prevalence of glaucoma and projections of glaucoma burden through 2040: a systematic review and meta-analysis. *Ophthalmology*, 121(11):2081–2090.
- Varma, R., Vajaranant, T. S., Burkemper, B., Wu, S., Torres, M., Hsu, C., Choudhury, F., and McKean-Cowdin, R. (2016). Visual impairment and blindness in adults in the united states: demographic and geographic variations from 2015 to 2050. *JAMA ophthalmology*, 134(7):802–809.
- Vijaya, L., George, R., Paul, P. G., Baskaran, M., Arvind, H., Raju, P., Ramesh, S. V., Kumaramanickavel, G., and McCarty, C. (2005). Prevalence of open-angle glaucoma in a rural south indian population. *Investigative ophthalmology & visual science*, 46(12):4461–4467.
- Walter, T., Klein, J.-C., Massin, P., and Erginay, A. (2002). A contribution of image processing to the diagnosis of diabetic retinopathy-detection of exudates in color fundus images of the human retina. *IEEE transactions on medical imaging*, 21(10):1236–1243.
- Wankhede, P. and Khanchandani, K. (2016). Optic disc detection using histogram based template matching. In *2016 International Conference on Signal Processing, Communication, Power and Embedded System (SCOPES)*, pages 182–185. IEEE.
- Weiss, J. M. (2008). Real-time feature detection using the hough transform. In *CAINE*, pages 168–173.
- Wong, D., Liu, J., Lim, J., Jia, X., Yin, F., Li, H., and Wong, T. (2008). Level-set based automatic cup-to-disc ratio determination using retinal fundus images in argali. In *2008 30th Annual International Conference of the IEEE Engineering in Medicine and Biology Society*, pages 2266–2269. IEEE.
- Wong, D. W. K., Liu, J., Tan, N. M., Yin, F., Lee, B.-H., and Wong, T. Y. (2010). Learning-based approach for the automatic detection of the optic disc in digital retinal fundus photographs. In *2010 Annual International Conference of the IEEE Engineering in Medicine and Biology*, pages 5355–5358. IEEE.
- Xiong, L. and Li, H. (2016). An approach to locate optic disc in retinal images with pathological changes. *Computerized Medical Imaging and Graphics*, 47:40–50.
- Xu, D. and Tian, Y. (2015). A comprehensive survey of clustering algorithms. *Annals of Data Science*, 2(2):165–193.
- Yang, X.-S. (2010). *Nature-inspired metaheuristic algorithms*. Luniver press.
- Yin, F., Liu, J., Ong, S. H., Sun, Y., Wong, D. W., Tan, N. M., Cheung, C., Baskaran, M., Aung, T., and Wong, T. Y. (2011). Model-based optic nerve head segmentation on retinal fundus images. In *2011 Annual International Conference of the IEEE Engineering in Medicine and Biology Society*, pages 2626–2629. IEEE.

- Youssif, A. A.-H. A.-R., Ghalwash, A. Z., and Ghoneim, A. A. S. A.-R. (2008). Optic disc detection from normalized digital fundus images by means of a vessels' direction matched filter. *IEEE transactions on medical imaging*, 27(1):11–18.
- Zhang, D. and Zhao, Y. (2016). Novel accurate and fast optic disc detection in retinal images with vessel distribution and directional characteristics. *IEEE journal of biomedical and health informatics*, 20(1):333–342.
- Zhu, X. and Rangayyan, R. M. (2008). Detection of the optic disc in images of the retina using the hough transform. In *2008 30th Annual International Conference of the IEEE Engineering in Medicine and Biology Society*, pages 3546–3549. IEEE.
- Zilly, J., Buhmann, J. M., and Mahapatra, D. (2017). Glaucoma detection using entropy sampling and ensemble learning for automatic optic cup and disc segmentation. *Computerized Medical Imaging and Graphics*, 55:28–41.